Progress In Electromagnetics Research B, Vol. 62, 63–86, 2015

Floquet Modal Analysis to Modelize and Study 2-D Planar Almost Periodic Structures in Finite and Infinite Extent with Coupled Motifs

Bilel Hamdi[1, 2, *], Taoufik Aguili[1], and Henri Baudrand[2]

Abstract—Studying of mutual coupling parameters between the antenna elements in an array environment has been considered as the subject of feature research. That is why, in this paper, we present a new Floquet modal analysis procedure for analyzing almost periodic structures. Accurate evaluation of the mutual coupling could be achieved by this analysis. It is shown how Floquet analysis can be exploited to study a finite array with arbitrary amplitude and linear phase distribution in both x-y directions including mutual coupling effects. Two different calculation methods of coupling coefficients between the array elements are presented, in spectral and spatial domains, to solve the suggested problem. For modeling the given structures, the moment method combined with Generalized Equivalent Circuit (MoM-GEC) is proposed. High gain in the running time and memory used is given using Floquet analysis. To validate this work, several examples are shown.

1. INTRODUCTION

Recently, almost periodic planar structures in 2D-dimensional case becomes the subject of important scientific research, in particular in defense and space applications, communication systems and electronics devices such as: phased array radar systems, Frequency selective surfaces (FSSs) applications, millimeter waves and optical wave regions (among the others, reflect-arrays, phased arrays and electromagnetic band-gap structures, leaky waves antenna ect.) [10, 15, 22, 23]. Many numerical techniques have been invested in this context, and their goal is to solve partial differential equations with periodic boundaries conditions, for instance the finite element method (FEM), the method of moment (MoM) and finite-difference time-domain (FDTD) [1, 15, 27].

In this paper, we need to calculate the mutual coupling parameters between antennas array in bi-dimensional configuration and to emphasize their effects [6, 8, 15]. Most studies prove that it is difficult to determine precise results in dealing the mutual coupling problems: element-by-element method and infinite periodic structure method [2, 8, 16]. To take coupling effects into consideration, a new Floquet modal analysis is required to decrease the complexity of the investigated problem [3, 7, 9, 14, 15, 17].

A number of works have been reported taking different radiating structures with spatial formulation to study 2-D periodic planar dipole antenna array [6, 8]. But this work considers a new original modal approach based on the Floquet's theorem to facilitate the treatment of this kind of structure [1, 3, 4, 21]. The modal description of the impressed field has been given in spectral domain one, and the radiated fields have discrete spectra in the wavenumber space. Then, the generalized Fourier series expansion is usually introduced to express the field components, and the analysis region will be restraint to a single periodicity cell [9, 11, 13, 14, 22].

An appropriate superposition of Floquet-periodic fields leads to an integral representation of the sought solution that needs a careful numerical treatment, the integration being performed over all the phase shifts inside one Brillouin domain [3, 13]. The field sources (e.g., located elements) arrangement

Received 16 November 2014, Accepted 19 January 2015, Scheduled 13 February 2015

* Corresponding author: Bilel Hamdi (Bilel.Hamdi@laplace.univ-tlse.fr).

[1] Laboratory of the Communication Systems, National Engineering School of Tunis, B.P. 37, Le Bélvedere 1002, Tunis, Tunisia.

[2] Laplace Laboratory, ENSEEIHT, 2 rue Camichel, 31071 Toulouse cedex 4, France.

follows the periodicity of the problem. Thus, as all Floquet approaches for periodic structures do, the modal techniques based on direct application of Floquet's expansion are useful (needful) [9, 13].

This modal analysis can show some fundamental properties of the impressed electromagnetic fields and present the Periodic Fourier Transform to approach the radiated problem of periodic structures in the spectral-domain [11, 14, 22]. For many periodic and almost periodic structures, several studies have proven that the method of moments (MoM) represents an appropriate and a rigorous numerical technique to compute the coupling between elements [1–3, 5, 16, 17].

In this work, we focus essentially on evaluating the electromagnetic interaction (the mutual coupling parameters) produced between the narrow array elements (e.g., conducting metallic shape) in two-dimensional periodic case. For solving this problem, we propose adopting an integral method based on the generalized equivalent model and using the Floquet modes written as a group of excitation sources. This proven Floquet modal technique allows to considerably reduce the running time and used memory observed by other conventional methods [1, 26].

This paper is structured as follows. The first step is to present the essential theoretical Floquet modal analysis. To begin with, the Finite Fourier Transform (FFT) and spectral decomposition are given. Next, in Section 3 the studied problem is formulated by an integral equation based on the formalism of the admittance (or impedance) operator using Generalized Equivalent Circuit (GEC) cited in [1, 3]. Then, in Section 4 numerical results are presented and discussed for many applications. Finally, in the last section some conclusions are drawn.

2. MODAL ANALYSIS

The study is devoted to explain the periodic assemblies of identical elements arranged in one-dimensional extent (configuration), then the bi-dimensional case can be easily given.

Using the modal analysis, the periodic symmetry of the structure allows us to concentrate on one cell of the array. The unit cell can be defined as the basic building block (can be an arbitrary metallic shape) of the array that repeats itself infinitely defined by the periodicity (d_x, d_y), as mentioned in Figure 1.

Generally, any periodic array can be excited in two ways: incident plane wave $E_{i,\alpha\beta}$ (passive array) or individual source connected to every elements (active array).

In this work, we are always interested in the active manner that a real voltage source (with uniform field) represents the excitation term associated with feeding element location connected to the radiating surface with arbitrary metallic shape.

This kind of source must also respect the property of the located element which should be smaller than the wavelength (dimensions are inferior to $\frac{\lambda}{10}$) in order to introduce a neglected phase shift. It is possible to express the excitation source by a non-uniform field [1, 20].

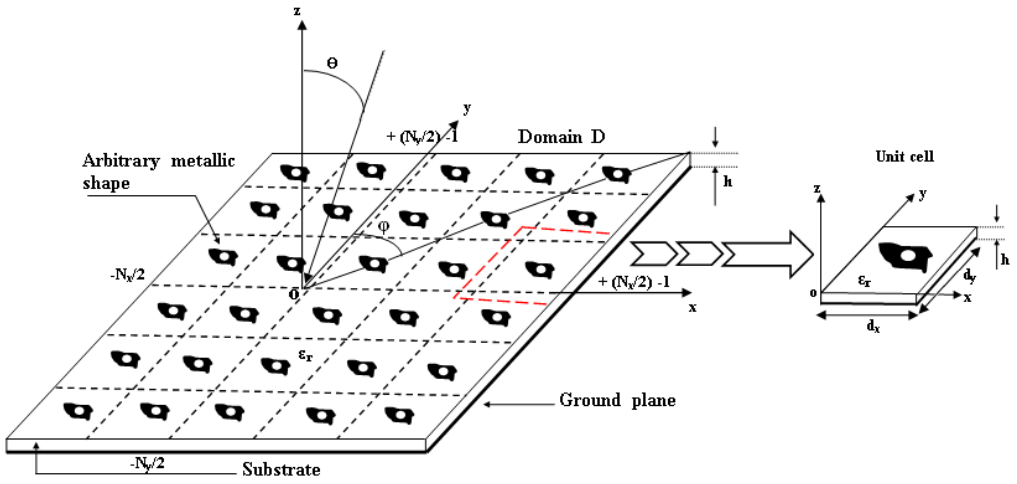

Figure 1. Periodic cells with arbitrary planar metallic shape (arbitrary motifs).

Based on Floquet states or Floquet eigen modes, we will identify all proper phases shift of the unit cell surrounded by others cells. The passage from each element to the other is provided through this phases.

The interaction and mutual coupling between cells are taken into account through the adequate periodic boundary conditions at the borders of the basic cell (Floquet's theorem).

Applying superposition theorem leads to predict mutual coupling parameters established between distinct elements which belong to the whole structure.

The determination of [**S**] matrix is more complex by using old spatial method (direct manner). To overcome this limitation, it is facile to estimate it by a simple elegant Fourier Transform based on Floquet's modes. A good accuracy is satisfied by this important mutual coupling expression.

The Floquet modal analysis, possibly, permits to study almost periodic structure with spatial irregularities. In the studied structure with periodicity character, we can find some cells with defects. Hence, each defect in any cell can be represented by replacing its source by an impedance surface to carry back the structure's geometry which has periodic symmetry, and cells become identical and uniform [10].

Note that this new modal study remains successfully valid for several geometries of radiating planar metallic shape in various periodic or aperiodic configurations.

As we have already seen, this efficient original modal analysis introduces a new way to decompose excitation source in spectral domain, which is applicable to finite and infinite periodic structures that remove the complexity of the problem under consideration to model and analyze the periodic structure when motifs are strongly or weakly coupled.

To make modal analysis more comprehensive, we should briefly remind the 1D-Fourier's principle of the feeding sources that easily provide explanation of the high-dimensional case with different periodicities and axis orientations especially for practical case of finite number of planar motif with arbitrary shape.

2.1. 1D-Fourier Transform's Principle of the Feeding Sources: Floquet's Theorem

This section, referring to [1], will describe the Floquet modal analysis and to show its detailed expressions in order to study the 1D-almost periodic array model in finite and infinite configurations.

2.2. 2D-Fourier Transform's Principle of the Feeding Sources: Floquet'S Theorem

In this section, to tackle all elements in 2D-configuration we propose to generalize the preceding case with more complex periodicities [1]. Consider a 2-D structure, linear array of point sources on the x-y plane with its (i, s)th element placed at $\overrightarrow{r_{is}} = (id_x, sd_y, 0)$ with $-\frac{N_x}{2} \leq i \leq \frac{N_x}{2} - 1$, $-\frac{N_y}{2} \leq s \leq \frac{N_y}{2} - 1$, d_x and d_y being the inter-element periods in the x and y coordinates, respectively. Add the second direction leads to two Floquet modes (α_p, β_q) in the modal space when each element is surrounded by suitable periodic walls along (ox) and (oy) directions [3].

As in the 1-D case, for a 2-D grid the source field $E(i, s)$ is decomposed as:

$$E(id_x, sd_y) = \frac{1}{\sqrt{N_x N_y}} \sum_{p=-\frac{N_x}{2}, q=-\frac{N_y}{2}}^{\frac{N_x}{2}-1, \frac{N_y}{2}-1} \tilde{E}_{\alpha_p, \beta_q} e^{j\alpha_p(id_x)} e^{j\beta_q(sd_y)} \tag{1}$$

Identically, the current distribution $J(i, s)$ is expressed as:

$$J(id_x, sd_y) = \frac{1}{\sqrt{N_x N_y}} \sum_{p=-\frac{N_x}{2}, q=-\frac{N_y}{2}}^{\frac{N_x}{2}-1, \frac{N_y}{2}-1} \tilde{J}_{\alpha_p, \beta_q} e^{j\alpha_p(id_x)} e^{j\beta_q(sd_y)} \tag{2}$$

with

$$\alpha_p = \frac{2\pi p}{L_x} \tag{3}$$

where

$$-\frac{N_x}{2} \leq p \leq \frac{N_x}{2} - 1 \tag{4}$$

and

$$L_x = N_x d_x \tag{5}$$

$$\beta_q = \frac{2\pi q}{L_y} \tag{6}$$

where

$$-\frac{N_y}{2} \leq q \leq \frac{N_y}{2} - 1 \tag{7}$$

and

$$L_y = N_y d_y \tag{8}$$

Like in the 1-D case, we rewrite the IFFT as follows:

$$\tilde{E}_{\alpha_p,\beta_q}(0) = \tilde{E}_{\alpha_p,\beta_q} = \frac{1}{\sqrt{N_x N_y}} \sum_{i=-\frac{N_x}{2},s=-\frac{N_y}{2}}^{\frac{N_x}{2}-1,\frac{N_y}{2}-1} E(id_x, sd_y) e^{-j\alpha_p(id_x)} e^{-j\beta_q(sd_y)} \tag{9}$$

and

$$\tilde{J}_{\alpha_p,\beta_q}(0) = \tilde{E}_{\alpha_p,\beta_q} = \frac{1}{\sqrt{N_x N_y}} \sum_{i=-\frac{N_x}{2},s=-\frac{N_y}{2}}^{\frac{N_x}{2}-1,\frac{N_y}{2}-1} J(id_x, sd_y) e^{-j\alpha_p(id_x)} e^{-j\beta_q(sd_y)} \tag{10}$$

Similar to the 1D-case, the 2-D periodic structure is a group of (N_x, N_y) identical phased cells, where the exponential term $e^{-j\alpha_p(id_x)\beta_q(sd_y)}$ indicates the phase term for each (i, s)th cell at each mode (α_p, β_q).

Following the same 1D-Fourier Transform's vector-matrix notation, we would like to put emphasis on a new mutual coupling relationship that follows the 2D-lattice arrays. We also need to reconstruct a 2D-Fourier matrix that identify all the same properties of the 1D-Fourier matrix to finally deduce the main expression given below:

$$[Z_{i,s}] = TF^{-1}[\tilde{z}_{\alpha_p,\beta_q}]TF \tag{11}$$

We have seen that $\tilde{z}_{\alpha_p,\beta_q}$ is a diagonal operator which contains all possible modal input impedances. The consequence of this latter transformation is to deduce the mutual admittance and the scattering parameters between periodic elements in an array environment that may be defined as:

$$[Y_{i,s}] = TF^{-1}[\tilde{y}_{\alpha_p,\beta_q}]TF \tag{12}$$

$$[S_{i,s}] = TF^{-1}[\tilde{s}_{\alpha_p,\beta_q}]TF \tag{13}$$

3. PROBLEM FORMULATION

This section presents two different formulations to analyze the theoretical development appreciably for solving planar structure in periodic arrays:

- The modal formulation restraint to modelize the unit structure that is designed to show the dependence on Floquet modes.
- As we know, it is important to explain, also, the old spatial formulation associated to the whole structure.

3.1. Modal Formulation

Owing to the generalized equivalent approach, the integral equation representation can be expressed by the unit equivalent circuit that the Kirchhoff laws are employed. The generalized test functions which describe the electromagnetic state on the discontinuity plane are modeled by an adjustable virtual source

not storing energy (unknown current density).

The excitation term is depicted within the GEC using a field source or a current source (located element).

Consider that the environment of the unit structure is expressed by an impedance (or an admittance) operator corresponding to evanescent modes.

We should bear in mind that the $\hat{Z}_{\alpha,\beta}$ expression following the Dirac notation is then rewritten as:

$$\left[\hat{Z}^{upper,down}_{pq,ht,\alpha\beta}\right] = \left[\sum_{m,n} \langle g_{pq,\alpha\beta}|f_{mn,\alpha\beta}\rangle z^{upper,down}_{mn,\alpha\beta} \langle f_{mn,\alpha\beta}|g_{ht,\alpha\beta}\rangle\right] \tag{14}$$

and the inner product is given by:

$$\langle u|v\rangle = \int\int_D uv^*\, ds \tag{15}$$

(* denotes the complex conjugate), $|f_{mn,\alpha\beta}\rangle$ represent the modes $|TE_{mn,\alpha\beta}\rangle$ and $|TM_{mn,\alpha\beta}\rangle$.

Here we will define the known expression of $|f^{TE,TM}_{mn,\alpha\beta}\rangle$ functions that identify 2-D periodic walls as [3]:

$$\left\{\begin{array}{l} |TE_{mn,\alpha\beta}\rangle \\ m \in Z^* \\ n \in N^* \end{array}\right\} = \left\{\begin{array}{l} j\dfrac{k_{yn}}{\sqrt{k^2_{xm,\alpha}+k^2_{yn}}}\sqrt{\dfrac{1}{d_x d_y}} \\ \exp(+j(k_{xm,\alpha}x))\exp(+j(k_{yn,\beta}y) \\ -j\dfrac{k_{xm,\alpha}}{\sqrt{k^2_{xm,\alpha}+k^2_{yn}}}\sqrt{\dfrac{1}{d_x d_y}} \\ \exp(+j(k_{xm,\alpha}x))\exp(+j(k_{yn,\beta}y) \end{array}\right. \tag{16}$$

$$\left\{\begin{array}{l} |TM_{mn,\alpha\beta}\rangle \\ m \in Z^* \\ n \in N^* \end{array}\right\} = \left\{\begin{array}{l} j\dfrac{k_{xm,\alpha}}{\sqrt{k^2_{xm,\alpha}+k^2_{yn}}}\sqrt{\dfrac{1}{d_x d_y}} \\ \exp(+j(k_{xm,\alpha}x))\exp(+j(k_{yn,\beta}y) \\ j\dfrac{k_{yn}}{\sqrt{k^2_{xm,\alpha}+k^2_{yn}}}\sqrt{\dfrac{1}{d_x d_y}} \\ \exp(+j(k_{xm,\alpha}x))\exp(+j(k_{yn,\beta}y) \end{array}\right. \tag{17}$$

$$\left\{\begin{array}{l} |TEM_{\alpha\beta}\rangle \\ m=0 \\ n=0 \end{array}\right\} = \left\{\begin{array}{l} |TE_{00,\alpha\beta}\rangle \\ m=0 \\ n=0 \end{array}\right\} = \left\{\begin{array}{l} j\dfrac{\beta}{\sqrt{\alpha^2+\beta^2}}\sqrt{\dfrac{1}{d_x d_y}} \\ \exp(+j(\alpha x))\exp(+j(\beta y) \\ -j\dfrac{\alpha}{\sqrt{\alpha^2+\beta^2}}\sqrt{\dfrac{1}{d_x d_y}} \\ \exp(+j(\alpha x))\exp(+j(\beta y) \end{array}\right. \tag{18}$$

$$\left\{\begin{array}{l} |TEM_{\alpha\beta}\rangle \\ m=0 \\ n=0 \end{array}\right\} = \left\{\begin{array}{l} |TM_{00,\alpha\beta}\rangle \\ m=0 \\ n=0 \end{array}\right\} = \left\{\begin{array}{l} j\dfrac{\beta}{\sqrt{\alpha^2+\beta^2}}\sqrt{\dfrac{1}{d_x d_y}} \\ \exp(+j(\alpha x))\exp(+j(\beta y) \\ j\dfrac{\alpha}{\sqrt{\alpha^2+\beta^2}}\sqrt{\dfrac{1}{d_x d_y}} \\ \exp(+j(\alpha x))\exp(+j(\beta y) \end{array}\right. \tag{19}$$

$k_{xm,\alpha} = \frac{2m\pi}{d_x} + \alpha$ and $k_{yn,\beta} = \frac{2m\pi}{d_y} + \beta$ are wavenumbers.

For the normal incidence, there are two modes TEM (TE_{00} or TM_{00}) which can be expressed as: $|TEM\rangle = \sqrt{\frac{1}{d_x d_y}}\overrightarrow{x}$ or $|TEM\rangle = \sqrt{\frac{1}{d_x d_y}}\overrightarrow{y}$

For a 1-D structure, we will specify a new expression of $|f_{mn,\alpha}^{TE,TM}\rangle$ functions, combining electric-periodic walls or magnetic-periodic walls (see Appendix A) [1].

By applying the local form of Maxwell equations and verifying $\langle f_{mn,\alpha\beta}|f_{m',n',\alpha\beta}\rangle = \delta_{m,n}^{m',n'}$ (the Kronecker symbol), we can be sure that this new basis functions obey: $\overrightarrow{rot}(\overrightarrow{E}) = -j\mu\omega\overrightarrow{H}$ and $\mathrm{div}(\overrightarrow{E}) = -j\beta E_z$, precisely:

For $|TM_{mn,\alpha\beta}\rangle$ the: $\begin{cases} H_z = 0 \\ E_z \neq 0 \end{cases} \Rightarrow \overrightarrow{rot}(|TM_{mn,\alpha\beta}\rangle) = \overrightarrow{0}$

For $|TE_{mn,\alpha\beta}\rangle$ the: $\begin{cases} E_z = 0 \\ H_z \neq 0 \end{cases} \Rightarrow div(|TE_{mn,\alpha\beta}\rangle) = 0$

$\tilde{z}_{mn,\alpha\beta}$ the total modal impedance associated with these vectors can be expressed as:

$$\tilde{z}_{mn,\alpha\beta,upper}^{TE} = \frac{j\omega\mu_0}{\gamma^2(k_{xm,\alpha}, k_{yn,\beta})} \tag{20}$$

$$\tilde{z}_{mn,\alpha\beta,upper}^{TM} = \frac{\gamma^2(k_{xm,\alpha}, k_{yn,\beta})}{j\omega\epsilon_0} \tag{21}$$

$$\gamma^2(k_{xm,\alpha}, k_{yn,\beta}) = k_{xm,\alpha}^2 + k_{yn,\beta}^2 - k^2 \tag{22}$$

And

$$\tilde{z}_{mn,\alpha\beta,down}^{TE} = \frac{j\omega\mu_0}{\gamma^2(k_{xm,\alpha}, k_{yn,\beta})} \tanh(\gamma(k_{xm,\alpha}, k_{yn,\beta})h) \tag{23}$$

$$\tilde{z}_{mn,\alpha\beta,down}^{TM} = \frac{\gamma^2(k_{xm,\alpha}, k_{yn,\beta})}{j\omega\epsilon_r\epsilon_0} \tanh(\gamma(k_{xm,\alpha}, k_{yn,\beta})h) \tag{24}$$

$$\gamma^2(k_{xm,\alpha}, k_{yn,\beta}) = k_{xm,\alpha}^2 + k_{yn,\beta}^2 - \epsilon_r k^2 \tag{25}$$

$$K = 2\pi f\sqrt{\epsilon_r\epsilon_0\mu_0} \tag{26}$$

A particular choice of the trial functions which describe the unknown current density is defined on the metallic parts of the unit cell.

$|g_{pq,\alpha\beta}\rangle$ designates a trial function and $X_{pq,\alpha\beta}$ the unknown coefficients of this function to be determined.

The discontinuity plane can be composed of a metallic surface and a dielectric surface. The unknown virtual current source $\tilde{J}_{e,\alpha\beta}$ is defined on the metallic surface and is null on the dielectric part. We note $\tilde{E}_{\alpha\beta}$ its dual.

Based on GEC method and using impedance's operator representation, we can identify the relationship between the electric field and the current density. Then, the theoretical development as done for the unit cell leads to expressing the modal input impedance for any Floquet mode as stated in (27).

$$\tilde{Z_{in,\alpha\beta}} = \left({}^t[\tilde{A}_{\alpha\beta}]([\hat{Z}_{pq,ht,\alpha\beta}^{down}]^{-1} + [\hat{Z}_{pq,ht,\alpha\beta}^{upper}]^{-1})[\tilde{A}_{\alpha\beta}]\right)^{-1} \tag{27}$$

where

$$[\tilde{A}_{\alpha\beta}] = [\langle f|g_{pq,\alpha\beta}\rangle] = [\langle\frac{1}{\delta}|g_{pq,\alpha\beta}\rangle] \tag{28}$$

Consider the circuit example shown in Figure 2. Applying the kirchhoff's laws (current and tension's laws), we can deduce the relation between virtual and real sources and its duals, as given in the following system:

$$\begin{cases} \tilde{J}_{\alpha\beta} = \tilde{J}_{e,\alpha\beta} \\ \tilde{E}_{e,\alpha\beta} = -\tilde{E}_{\alpha\beta} + \hat{Z}_{\alpha\beta}\tilde{J}_{e,\alpha\beta} \end{cases} \tag{29}$$

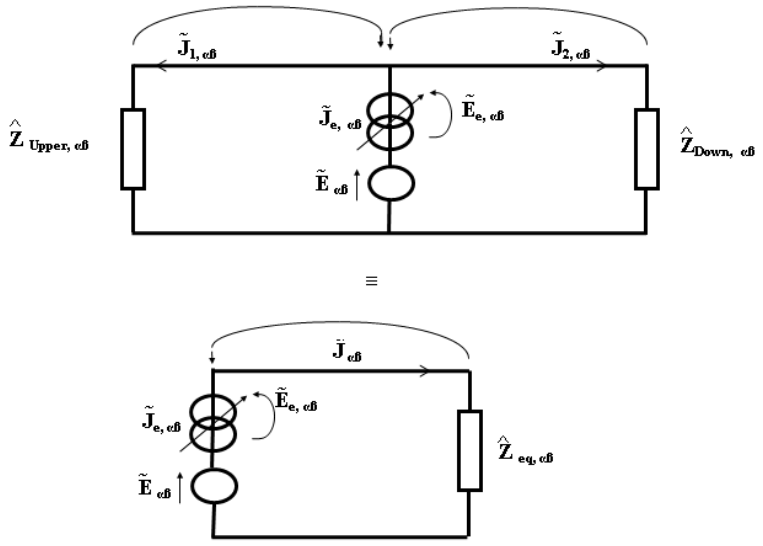

Figure 2. Equivalent circuit for the unit cell.

Thus, we can determine the current density lying in the metal part including the source domain and its associated field to verify the boundary conditions.

Next, the integral equation is solved on the central element by applying the MoM method using Galerkin procedure. Taking now into account that the original periodic excitation was written as a combination of Floquet-periodic impressed fields by means of the linear transformation cited in [1, 3, 4], after applying the superposition principle, the current density excited by the located source on the periodic micro-strip line can be finally computed as [3, 9, 17]:

$$J(x,y) = \frac{(d_x d_y)}{4\pi^2} \int_{\frac{-\pi}{d_x}}^{\frac{\pi}{d_x}} \int_{\frac{-\pi}{d_y}}^{\frac{\pi}{d_y}} \tilde{J}_{\alpha\beta}(x,y)\, d\alpha\ d\beta \tag{30}$$

Similarly, we express the superposition theorem:

$$J(x,y) = \frac{1}{\sqrt{N_x N_y}} \sum_{p,q} \tilde{J}_{\alpha_p,\beta_q}(x,y) \tag{31}$$

To formulate 1-D extent described in [1], we reduce the doubly periodic grid on one axis (one translation vector) whose motifs follow the 1-D periodic arrangement and the Floquet dependence is also reduced to a single direction that delete the second phase corresponding to β dependence.

3.2. Spatial Formulation

Another classical way permits to study the whole or the global 2-D structure separately based on the old spatial formulation [6].

As the proposed formulation in [1], we describe the direct manner that extracts an integral equation to compute the impedance matrix which represents also the mutual impedance. This main relation can be compared with the given Equation (11) obtained by the Fourier Transform.

Let's take an uniform and identical located sources will excite respectively every metallic shape that belongs to the whole array configuration. Their generalized equivalent circuits model, which allows to simplify the Maxwell equations and the continuity relations, is shown in Figure 3 [12, 18, 19, 25].

Consider $|f_{mn}^{TE,TM}\rangle$ the modes (or basis functions) of the proposed waveguide enclosing reference structure (see Figure 4).

Lateral walls can be chosen from the following known options: (a) Perfect Electric boundaries, (b) Perfect Magnetic boundaries, (c) Periodic boundaries with null phases shift, or (d) a combination of

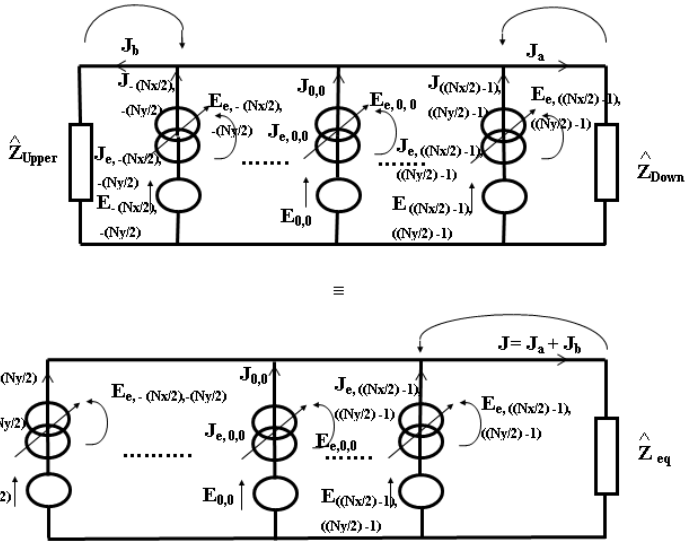

Figure 3. Equivalent circuit for the global structure.

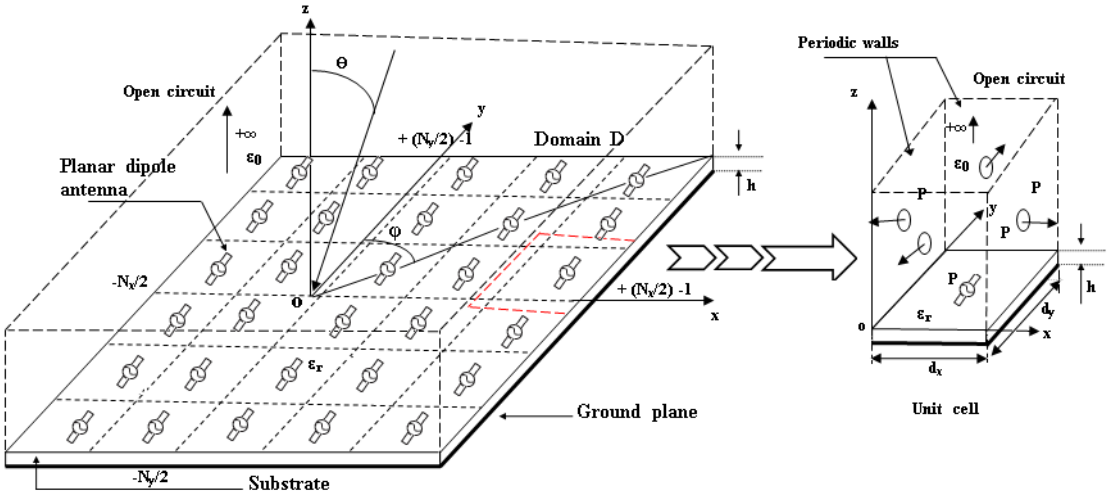

Figure 4. Periodic cells with printed dipoles antenna.

these latter boundary conditions (see Appendix B). The top and the bottom are an open circuit and a ground plane, respectively.

The excitation fields $E_{i,s}$,$(i,s) \in ([-\frac{N_x}{2}, \frac{N_x}{2}-1], [-\frac{N_y}{2}, \frac{N_y}{2}-1])$ are expressed as follows $E_{i,s} = V_i f_{i,s}$ where $f_{i,s} = \frac{1}{\delta}$ represents the fundamental excitations modes.

The impedance operator $\hat{Z}$ expressed as a function of higher-order modes and their modes impedances $z_{mn}^{TE,TM}$. The unknown of the problem $J_e^{i,s}$ describes the virtual current appearing on each metal part and represents the electromagnetic state on the discontinuity interface.

So, $J_e^{i,s}$ is expressed as a series of known test functions $g_{pq}^{i,s}$ weighted by unknown coefficients.

Based on its corresponding equivalent circuit model depicted in Figure 3, the generalized Ohm and Kirchhoff laws are then rewritten as an equations system:

$$\begin{cases} J_{(i,s)} = J_{e,(i,s)} \\ E_{e,(i,s)} = -E_{i,s} + \hat{Z}J \end{cases} \tag{32}$$

with:

$$J = J_{e,(-\frac{N_x}{2},-\frac{N_y}{2})} + J_{e,(-\frac{N_x}{2}+1,-\frac{N_y}{2}+1)} + \ldots + J_{e,(\frac{N_x}{2}-1,\frac{N_y}{2}-1)} = J_{-\frac{N_x}{2},-\frac{N_y}{2}} + J_{-\frac{N_x}{2}+1,-\frac{N_y}{2}+1} + \ldots + J_{\frac{N_x}{2}-1,\frac{N_y}{2}-1} \tag{33}$$

A formal relation between sources (real and virtual) and their duals is given in (34):

$$\begin{pmatrix} J_{-\frac{N_x}{2},-\frac{N_y}{2}} \\ . \\ . \\ J_{\frac{N_x}{2}-1,\frac{N_y}{2}-1} \\ \hline E_{e,(-\frac{N_x}{2},-\frac{N_y}{2})} \\ . \\ . \\ E_{e,(\frac{N_x}{2}-1,\frac{N_y}{2}-1)} \end{pmatrix} = \left(\begin{array}{cccc|cccc} 0 & . & . & 0 & 1 & 0 & . & 0 \\ 0 & . & . & 0 & 0 & 1 & 0 & . \\ 0 & . & . & 0 & . & 0 & 1 & 0 \\ 0 & . & . & 0 & 0 & . & 0 & 1 \\ \hline -1 & 0 & . & 0 & & & & \\ 0 & -1 & 0 & . & & & & \\ . & 0 & -1 & 0 & & \hat{Z_{pq,st}} & & \\ 0 & . & 0 & -1 & & & & \end{array}\right) \begin{pmatrix} E_{-\frac{N_x}{2},-\frac{N_y}{2}} \\ . \\ . \\ E_{\frac{N_x}{2}-1,\frac{N_x}{2}-1} \\ \hline J_{e,(-\frac{N_x}{2},-\frac{N_y}{2})} \\ . \\ . \\ J_{e,(\frac{N_x}{2}-1,\frac{N_y}{2}-1)} \end{pmatrix} \tag{34}$$

After that, we apply the Galerkin's procedure to Equation (34). Consequently, the impedance matrix $Z_{i,s}$ of the total structure (multi-port microwave circuits) is done as following:

$$[Z_{i,s}] = \left[\frac{V_{i,i}}{I_{s,s}}\right] = \left({}^{t}[A]([\hat{Z}^{down}_{pq,ht}]^{-1} + [\hat{Z}^{upper}_{pq,ht}]^{-1})[A]\right)^{-1} \tag{35}$$

where: $[A] = [\langle f_{i,s} | g^{i,s}_{pq,ht} \rangle]$, $[\hat{Z_{pq,ht}}] = [\langle g^{i,s}_{pq} | \hat{Z} | g^{i',s'}_{ht} \rangle]$, $(i,s) \in [-\frac{N_x}{2}, \frac{N_x}{2}-1][-\frac{N_y}{2}, \frac{N_y}{2}-1]$, $(i',s') \in [-\frac{N_x}{2}, \frac{N_x}{2}-1][-\frac{N_y}{2}, \frac{N_y}{2}-1]$ and $\hat{Z} = \sum_{m,n} |f^{TE,TM}_{mn}\rangle z^{upper,down}_{mn,TE,TM} \langle f^{TE,TM}_{mn}|$. Therefore, the mutual coupling effects in this case are expressed with the driving impedance matrix.

The latter Equation (35) relates these voltages $V_{i,i}$ and currents $I_{s,s}$ in the passive impedance case, so the matrix representation is written as:

$$[Z][I] = [V] \tag{36}$$

Identically, the admittance matrix, $[Y_{i,s}]$, is simply the inverse of the impedance matrix $[Z_{i,j}]$.

$$[Y_{i,s}] = [Z_{i,s}]^{-1} \tag{37}$$

The scattering parameters corresponding to the unique impedance matrix are deduced from the well-known form as the following [28]:

$$[S_{i,s}] = \left[\frac{Z_{i,s}}{Z_c} - I\right]\left[\frac{Z_{i,s}}{Z_c} + I\right]^{-1} \tag{38}$$

where Z_c is also the desired reference impedance of each element. For the example, if the matrix is re-normalized to 50 ohms, then (Z_c) will have value of $50\,\Omega$.

The suggested boundary conditions will be verified using the formulas (32) and (33) that produce the current densities lying in metal parts and their associated fields including the sources domains.

This formulation is extended further to study quasi-periodic circuits which leads to the appearance of leaky waves and their supporting role [23].

Their effects offer a precise information about mutual coupling terms. Especially, when the cental element (excited element) engenders a weak current distributions appearing on the others elements (no-excited elements).

In consequence, the previous modal formulation that focuses on analyzing the central cell is always applicable to structures with aperiodic configuration [3, 9, 13].

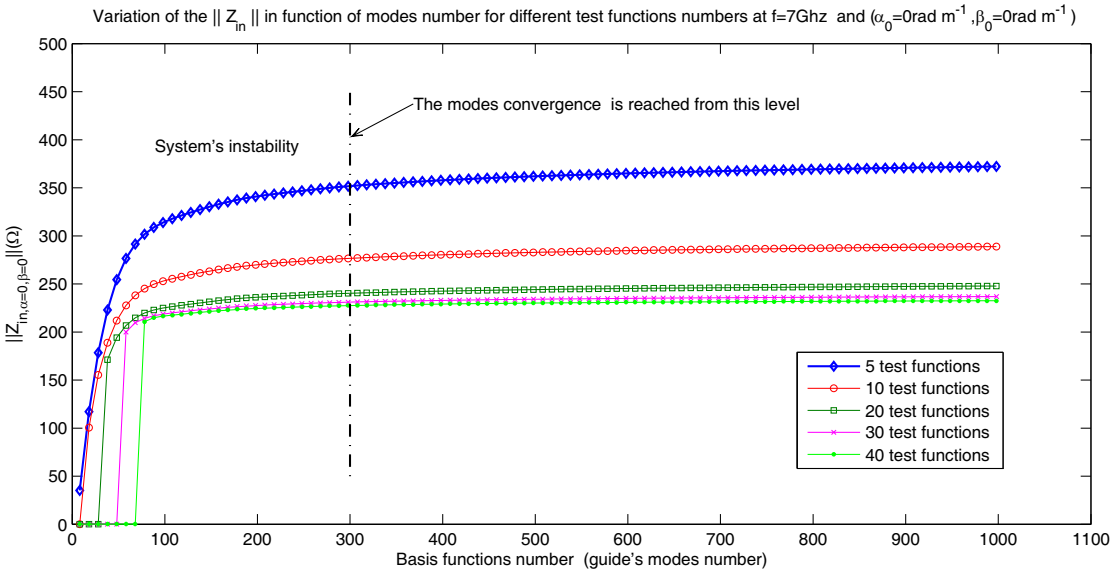

Figure 5. Variation of the $\|Z_{in,\alpha_0,\beta_0}\|$ in function of the guide's modes number for different test functions numbers at $f = 7\,\text{GHz}$ — The parameters which chosen to simulate the suggested unit structure are: $\alpha_0 = 0\,\text{rad m}^{-1}$, $\beta_0 = 0\,\text{rad m}^{-1}$, $w = 1\,\text{mm}$, $\delta = 0.75\,\text{mm}$ ($w \ll \lambda_0$, $\delta \ll \lambda_0$), $d_x = 108\,\text{mm}$, $d_y = 108\,\text{mm}$, $L = \lambda_0 \approx 54\,\text{mm}$, $h = 1.25\,\text{mm}$ and $\epsilon_r = 1$ (air).

4. NUMERICAL RESULTS: APPLICATIONS

For the verification and validation of simulation results, we propose the global structure under consideration, shown in Figure 4 and formed of finite (or infinite) periodic phased array planar conducting dipoles with their own excitations (arbitrary located voltage sources). All elements are bounded in a waveguide that the lateral walls are chosen among: (a) Perfect Electric boundaries, (b) Perfect Magnetic boundaries, (c) Periodic boundaries with null phases shift, or (d) a combination of these latter boundary conditions. The top and the bottom are respectively an open circuit and a ground plane. The unit structure is composed by an elementary planar dipole (conducting narrow), shielded in convenient periodic boundary conditions (rectangular dielectric waveguide). Also the top and the bottom are an open circuit and a ground plane. The considered planar circuits are lossless.

Initially, a good numerical convergence study is achieved, which is based on calculating the input impedance for each modal state using the Galerkin's procedure: Figures 6 and 5 prove how the convergence's peaks are reached when the test functions describing the metal part attain 40 test functions and when the levelled off modes appear from (300×300) basis functions.

This convergence study remains extended to other modal cases when $(\alpha_p \neq 0, \beta_q \neq 0)$.

Figure 7 represents the impedance Zin viewed by the excitation source calculated for the frequencies between [0–20] GHz to justify the electromagnetic quantity in (27). The behavior of Zin as a function of frequency allows determining the resonance frequency of the studied structure. These frequencies are in good agreement with the known electromagnetic response corresponding to classical thin wire dipoles. A good comparison with the ansoft HFSS is assured to validate our results. According to Figure 7, we can show the accuracy of our method compared to the Ansoft HFSS through the resonance frequency. For example, at the first resonance frequency $f = 5.1\,\text{GHz}$, we find an accuracy value about 1.9%. However, it becomes less than 1% in the rest of frequencies (outside the resonance frequencies). We think that the observed difference between the curves evaluated by the MoM-method and those simulated by the Ansoft HFSS tools is due to the badly matched the punctual excitation source defined by HFSS, in contrast to the planar source adopted by our method. Also, we have another manner given to verify the boundary conditions focused on representing the current density of the proposed structures.

Let's start by looking to the unit structure, as a consequence of which, we consider

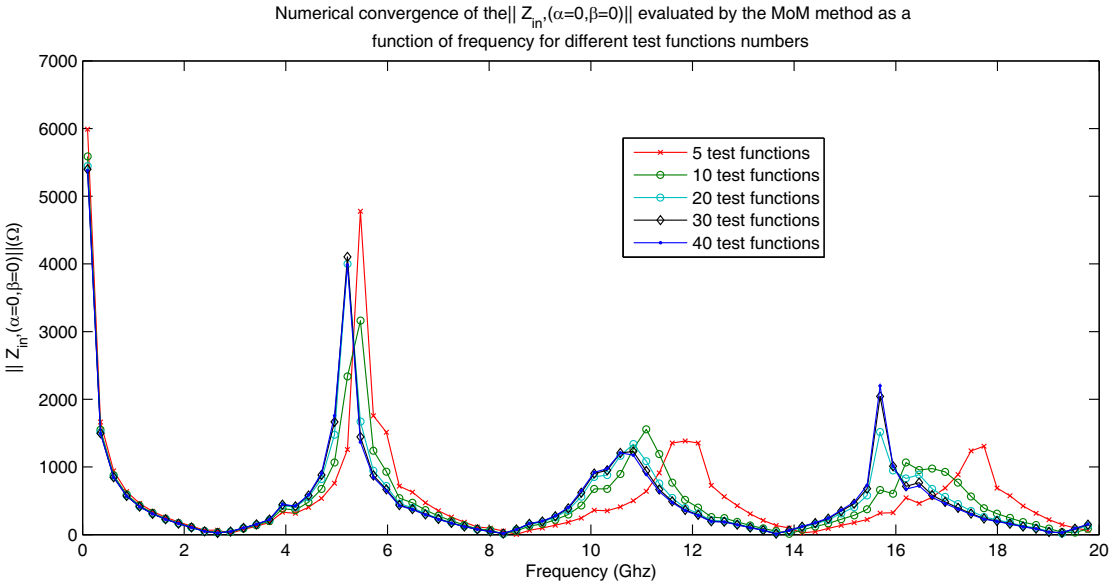

Figure 6. Numerical convergence of the $\|Z_{in,\alpha_0,\beta_0}\|$ evaluated by the MoM method as a function of frequency for different test functions numbers: $\alpha_0 = 0\,\text{rad m}^{-1}$, $\beta_0 = 0\,\text{rad m}^{-1}$, $w = 1\,\text{mm}$, $\delta = 0.75\,\text{mm}$ ($w \ll \lambda_0$, $\delta \ll \lambda_0$), $d_x = 108\,\text{mm}$, $d_y = 108\,\text{mm}$, $L = \lambda_0 \approx 54\,\text{mm}$, $h = 1.25\,\text{mm}$ and $\epsilon_r = 1$ (air).

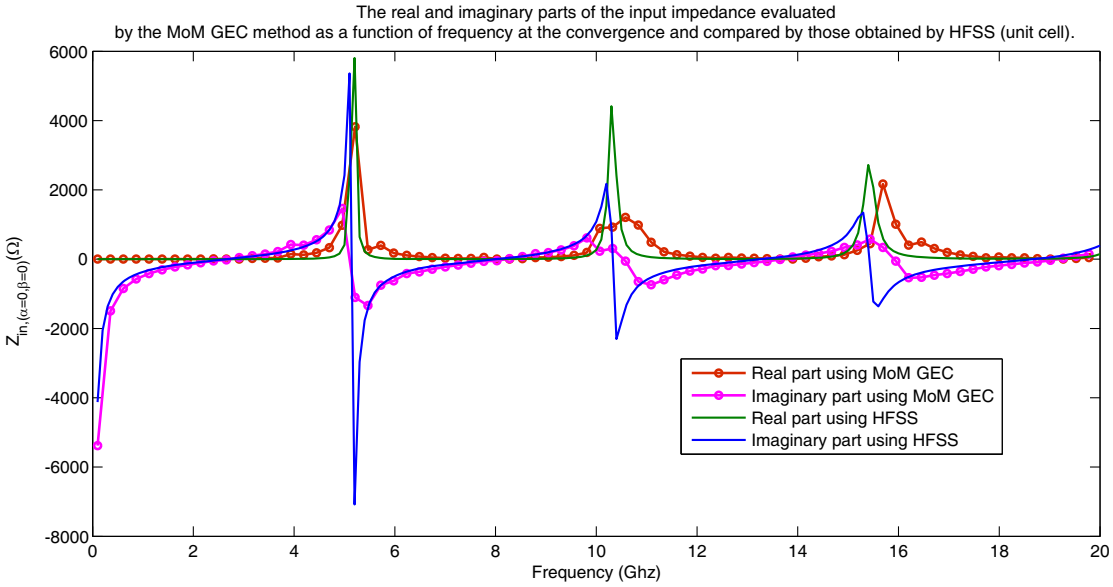

Figure 7. Evolution of the real and imaginary parts of the input impedance evaluated by the MoM method against the frequency at the convergence and compared by those obtained by HFSS (unit cell): $\alpha_0 = 0\,\text{rad m}^{-1}$, $\beta_0 = 0\,\text{rad m}^{-1}$, $w = 1\,\text{mm}$, $\delta = 0.75\,\text{mm}$ ($w \ll \lambda_0$, $\delta \ll \lambda_0$), $d_x = 108\,\text{mm}$, $d_y = 108\,\text{mm}$, $L = \lambda_0 \approx 54\,\text{mm}$, $h = 1.25\,\text{mm}$ and $\epsilon_r = 1$ (air).

Figures B1, B2, B3 and B4 to illustrate the current density evaluated by the MoM and obtained at the convergence conforming to the theory with consideration of the boundary conditions.

Further, we can add that it is considerably possible to identify the whole structure with the same manner that the current distributions in Figures B5, B6, B7, B8, B9, B10, B11, B12, B13 and B14 verify the boundary conditions where walls are periodic PPPP (with null phases shift) in the reference structure.

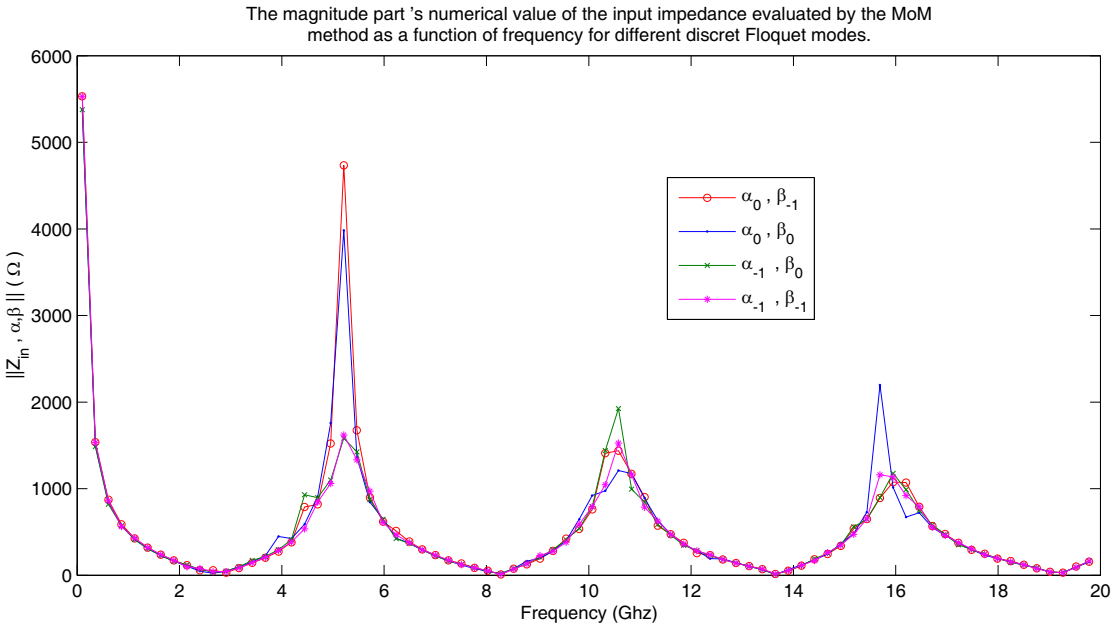

Figure 8. The magnitude part's numerical value of the input impedance evaluated by the MoM method as a function of frequency for different discret Floquet modes: $w = 1\,\text{mm}$, $\delta = 0.75\,\text{mm}$ ($w \ll \lambda_0$, $\delta \ll \lambda_0$), $d_x = 108\,\text{mm}$, $d_y = 108\,\text{mm}$, $L = \lambda_0 \approx 54\,\text{mm}$, $h = 1.25\,\text{mm}$ and $\epsilon_r = 1$ (air).

For any proposed configuration (structure), we remark that the current distributions provided respectively by the trial functions and the basis functions (guide's modes) are identical and have the same waves behaviour.

It is clear that the current distributions associated with the basis functions (guide's modes), as illustrated in Figures B1, B2, B5, B6, B7, B8, B9 and B10, prove that the Gibbs effects are practically suppressed when the convergence level is assured. These oscillations resulting from truncation are due to the Gibbs phenomenon. Because of this effect, we cannot write the boundary conditions in the immediate neighbourhood of the metal-dielectric plane [24, 25].

Figure 8 represents the magnitude part's numerical value of the input impedance behavior against the frequency for different discrete spectral values corresponding to a finite case composed of (2×2) elements in periodic array. It shows that the Floquet-input impedance considers the symmetry property especially in our case when Tables 1 and 2 prove that Z_{in,α_p,β_q} and $Z_{in,\alpha_{-p},\beta_{-q}}$ (or Z_{in,α_p,β_q} and $Z_{in,\alpha_{-p},\beta_q}$) are conformed to [7]. Then the edge effects are neglected.

Figure 8 shows that the mutual couplings are strong between elements only at the resonances which contain distinct values of modal impedances, whereas the rest of the frequencies are considered weak coupling. The identical cells are not coupled when the spatial period ($d \geq \lambda_0$) and the values of $Z_{in,\alpha,\beta}$ are practically constant and independent of (α, β) because the source is not sensitive to the boundary of each cell. Consequently, it appears that the $[\tilde{z}_{\alpha_p}, \beta_q]$ matrix is diagonal with identical terms. But, in our case to take into account mutual parameters in strong coupling, we should have a spatial periods ($d_x \leq \lambda_0$ and $d_y \leq \lambda_0$) which permit the modal input impedances that depend on the modal states (Floquet's modes) to appear obvious with a remarkable values.

Following this study we now define Tables 1 and 2 that contain possible spectral values (e.g., Finite structure) of the input impedance at $f = 5.4\,\text{GHz}$

Tables 1 and 2 permit us to deduce the mutual coupling parameters by using spectral representation: To validate this work, a good agreement with the spatial method is presented to calculate the scattering coupling parameters. Practically the [**S**] matrix has the same values when elements are strongly or weakly coupled as shown respectively in Tables 3, 4, 5 and 6.

The values of $S_{11}(db)$ are considered always poor due to the nature of the chosen motif which is

Table 1. Spectral input impedance at $f = 5.4\,\text{GHz}$ (finite case): $w = 1\,\text{mm}$, $\delta = 0.75\,\text{mm}$ ($w \ll \lambda_0$, $\delta \ll \lambda_0$), $d_x = d_y \approx 2\lambda_0 \approx 108\,\text{mm}$, $L = \lambda_0 \approx 54\,\text{mm}$, $(N_x \times N_y) = (2 \times 2)$ elements, $h = 1.25\,\text{mm}$ and $\epsilon_r = 1$ (air).

(p, q)	$(-1,-1)$	$(0,-1)$	$(-1,0)$	$(0,0)$
$(\alpha_p, \beta_q)(\text{radm}^{-1}, \text{radm}^{-1})$	$(\frac{-2\pi}{N_x d_x}, \frac{-2\pi}{N_y d_y})$	$(\frac{-2\pi}{N_x d_x}, 0)$	$(0, \frac{-2\pi}{N_y d_y})$	$(0, 0)$
$Z_{in}(\alpha_p, \beta_q)(\Omega)$	1588.4056–170.6839i	2520.3030–2859.3878i	1175.9366–590.0394i	609.3503–1737.1932i

Table 2. Spectral input impedance at $f = 5.4\,\text{GHz}$ (finite case): $w = 1\,\text{mm}$, $\delta = 0.75\,\text{mm}$ ($w \ll \lambda_0$, $\delta \ll \lambda_0$), $d_x = d_y \approx 2\lambda_0 \approx 108\,\text{mm}$, $L = \lambda_0 \approx 54\,\text{mm}$, $(N_x \times N_y) = (3 \times 3)$ elements, $h = 1.25\,\text{mm}$ and $\epsilon_r = 1$ (air).

(p, q)	$(-1,-1)$	$(-1,0)$	$(-1,+1)$	$(0,-1)$
$(\alpha_p, \beta_q)(\text{radm}^{-1}, \text{radm}^{-1})$	$(\frac{-2\pi}{N_x d_x}, \frac{-2\pi}{N_y d_y})$	$(\frac{-2\pi}{N_x d_x}, 0)$	$(\frac{-2\pi}{N_x d_x}, \frac{+2\pi}{N_y d_y})$	$(0, \frac{-2\pi}{N_y d_y})$
$Z_{in}(\alpha_p, \beta_q)(\Omega)$	1356.2119–491.7912i	433.3115–758.7562i	1356.2119–491.7912i	1316.3299–2393.7796i
$\hookrightarrow (0,0)$	$(0,+1)$	$(+1,-1)$	$(+1,0)$	$(+1,+1)$
$\hookrightarrow (0,0)$	$(0, \frac{+2\pi}{N_y d_y})$	$(\frac{+2\pi}{N_x d_x}, \frac{-2\pi}{N_y d_y})$	$(\frac{+2\pi}{N_x d_x}, 0)$	$(\frac{+2\pi}{N_x d_x}, \frac{+2\pi}{N_y d_y})$
609.3503–1737.1932i	1316.3299–2393.7796i	1356.2119–491.7912i	433.3115–758.7562i	1356.2119–491.7912i

Table 3. Mutual coupling parameters $S_{is}(db)$ between the array elements obtained using spectral formulation (or modal representation based on Floquet's modes) at $f = 5.4\,\text{GHz}$: $w = 1\,\text{mm}$, $\delta = 0.75\,\text{mm}$ ($w \ll \lambda_0$, $\delta \ll \lambda_0$), $d_x = d_y \approx 2\lambda_0 \approx 108\,\text{mm}$, $L = \lambda_0 \approx 54\,\text{mm}$, $(N_x \times N_y) = (2 \times 2)$ elements, $h = 1.25\,\text{mm}$, $Z_c = 50\,\Omega$ and $\epsilon_r = 1$ (air).

-0.3581	-32.4441	-36.9144	-55.3990
-32.4441	-0.3581	-55.3990	-36.9144
-36.9144	-55.3990	-0.3581	-32.4441
-55.3990	-36.9144	-32.4441	-0.3581

Table 4. Mutual coupling parameters $S_{is}(db)$ between the array elements obtained using spatial formulation at $f = 5.4\,\text{GHz}$ and ($\alpha_0 = 0\,\text{rad m}^{-1}$, $\beta_0 = 0\,\text{rad m}^{-1}$): $w = 1\,\text{mm}$, $\delta = 0.75\,\text{mm}$ ($w \ll \lambda_0$, $\delta \ll \lambda_0$), $d_x = d_y \approx 2\lambda_0 \approx 108\,\text{mm}$, $a = 216\,\text{mm}$, $b = 216\,\text{mm}$, $L = \lambda_0 \approx 54\,\text{mm}$, $(N_x \times N_y) = (2 \times 2)$ elements, $h = 1.25\,\text{mm}$, $Z_c = 50\,\Omega$ and $\epsilon_r = 1$ (air).

-0.2832	-36.1374	-50.9319	-55.8204
-36.1374	-0.2832	-55.8204	-50.9319
-50.9319	-55.8204	-0.2832	-36.1374
-55.8204	-50.9319	-36.1374	-0.2832

attached to (or placed near) the ground plane that permits to emit a maximum of radiating power when the transfer power between elements is assured.

Following Tables 1 and 2, considering the (α, β) values, Floquet harmonics may appear as an evanescent or propagating waves [22] which engender a scan blindness phenomena. This explains why we need to draw the Floquet modes and surface wave mode circles [7].

Table 5. Mutual coupling parameters $S_{is}(db)$ between the center element and other elements obtained using spectral formulation (or modal representation based on Floquet's modes) at $f = 5.4\,\text{GHz}$: $w = 1\,\text{mm}$, $\delta = 0.75\,\text{mm}$ ($w \ll \lambda_0$, $\delta \ll \lambda_0$), $d_x = d_y \approx 2\lambda_0 \approx 108\,\text{mm}$, $L = \lambda_0 \approx 54\,\text{mm}$, $(N_x \times N_y) = (3 \times 3)$ elements, $h = 1.25\,\text{mm}$, $Z_c = 50\,\Omega$ and $\epsilon_r = 1$ (air).

−0.4142	−34.8885	−34.8885	−36.5630	−44.5990	−44.5990	−36.5630	−44.5990	−44.5990
−34.8885	−0.4142	−34.8885	−44.5990	−36.5630	−44.5990	−44.5990	−36.5630	−44.5990
−34.8885	−34.8885	−0.4142	−44.5990	−44.5990	−36.5630	−44.5990	−44.5990	−36.5630
−36.5630	−44.5990	−44.5990	−0.4142	−34.8885	−34.8885	−36.5630	−44.5990	−44.5990
−44.5990	−36.5630	−44.5990	−34.8885	**−0.4142**	−34.8885	−44.5990	−36.5630	−44.5990
−44.5990	−44.5990	−36.5630	−34.8885	−34.8885	−0.4142	−44.5990	−44.5990	−36.5630
−36.5630	−44.5990	−44.5990	−36.5630	−44.5990	−44.5990	−0.4142	−34.8885	−34.8885
−44.5990	−36.5630	−44.5990	−44.5990	−36.5630	−44.5990	−34.8885	−0.4142	−34.8885
−44.5990	−44.5990	−36.5630	−44.5990	−44.5990	−36.5630	−34.8885	−34.8885	−0.4142

Table 6. Mutual coupling parameters $S_{is}(db)$ between the center element and other elements obtained using spatial formulation at $f = 5.4\,\text{GHz}$ and ($\alpha_0 = 0\,\text{rad m}^{-1}$, $\beta_0 = 0\,\text{rad m}^{-1}$): $w = 1\,\text{mm}$, $\delta = 0.75\,\text{mm}$ ($w \ll \lambda_0$, $\delta \ll \lambda_0$), $d_x = d_y \approx 2\lambda_0 \approx 108\,\text{mm}$, $a = 324\,\text{mm}$, $b = 324\,\text{mm}$, $L = \lambda_0 \approx 54\,\text{mm}$, $(N_x \times N_y) = (3 \times 3)$ elements, $h = 1.25\,\text{mm}$, $Z_c = 50\,\Omega$ and $\epsilon_r = 1$ (air).

−0.3081	−41.3058	−41.3058	−40.6364	−43.1792	−43.1792	−40.6364	−43.1792	−43.1792
−41.3058	−0.3081	−41.3058	−43.1792	−40.6364	−43.1792	−43.1792	−40.6364	−43.1792
−41.3058	−41.3058	−0.3081	−43.1792	−43.1792	−40.6364	−43.1792	−43.1792	−40.6364
−40.6364	−43.1792	−43.1792	−0.3081	−41.3058	−41.3058	−40.6364	−43.1792	−43.1792
−43.1792	−40.6364	−43.1792	−41.3058	**−0.3081**	−41.3058	−43.1792	−40.6364	−43.1792
−43.1792	−43.1792	−40.6364	−41.3058	−41.3058	−0.3081	−43.1792	−43.1792	−40.6364
−40.6364	−43.1792	−43.1792	−40.6364	−43.1792	−43.1792	−0.3081	−41.3058	−41.3058
−43.1792	−40.6364	−43.1792	−43.1792	−40.6364	−43.1792	−41.3058	−0.3081	−41.3058
−43.1792	−43.1792	−40.6364	−43.1792	−43.1792	−40.6364	−41.3058	−41.3058	−0.3081

5. STORAGE MEMORY AND TIME CONSUMING

In this section, we evaluate the Floquet modal formulation compared to the old spatial formulation in requirement memory cost and reducing computational time. To compute the mutual coupling parameters, as we know the used MoM-method necessitates a $(P \times P)$ matrix inversion, with P being the number of the test functions (descretization functions). In fact, the storage memory and the operation number of the conventional MoM depend on P as:

$$\begin{aligned} Storage &\approx O(P^2) \\ Noperation &\approx O(P^3) \end{aligned} \tag{39}$$

As we have always explained in our past work [1], we show how Floquet analysis is more important in terms of consuming time and memory resources. Moreover, the reduction of the unknowns's number results in minimizing the demanded computational resources. Furthermore, we denote T_{MoM} as the total time required by the spatial formulation to calculate the impedance matrix (mutual impedance).

$$T_{MoM} = M((N_x N_y)P)^2(T_s + T_{op}) + \frac{2}{3}((N_x N_y)P)^3 T_{op} + \delta \tag{40}$$

The term $M((N_x N_y)P)^2(T_s + T_{op})$ represents the needed time for matrix filling.

The term $\frac{2}{3}((N_x N_y)P)^3$ is associated with the impedance matrix inversion.

To compute the mutual coupling using the Fourier transformations and the Floquet analysis, we can write the total needed time by using the modal formulation as:

$$T_{MoM} = M(N_x N_y)(P)^2(T_s + T_{op}) + \frac{2}{3}(N_x N_y)(P)^3 T_{op} + \delta \tag{41}$$

where M is the total guide's modes number, $(N_x N_y)$ the number of printed dipoles, T_s the mean required time to compute a scalar product, T_{op} the mean needed time for an elementary operation (multiplication or addition), and δ a term which expresses the neglected residue including, for example, the time for filling matrix.

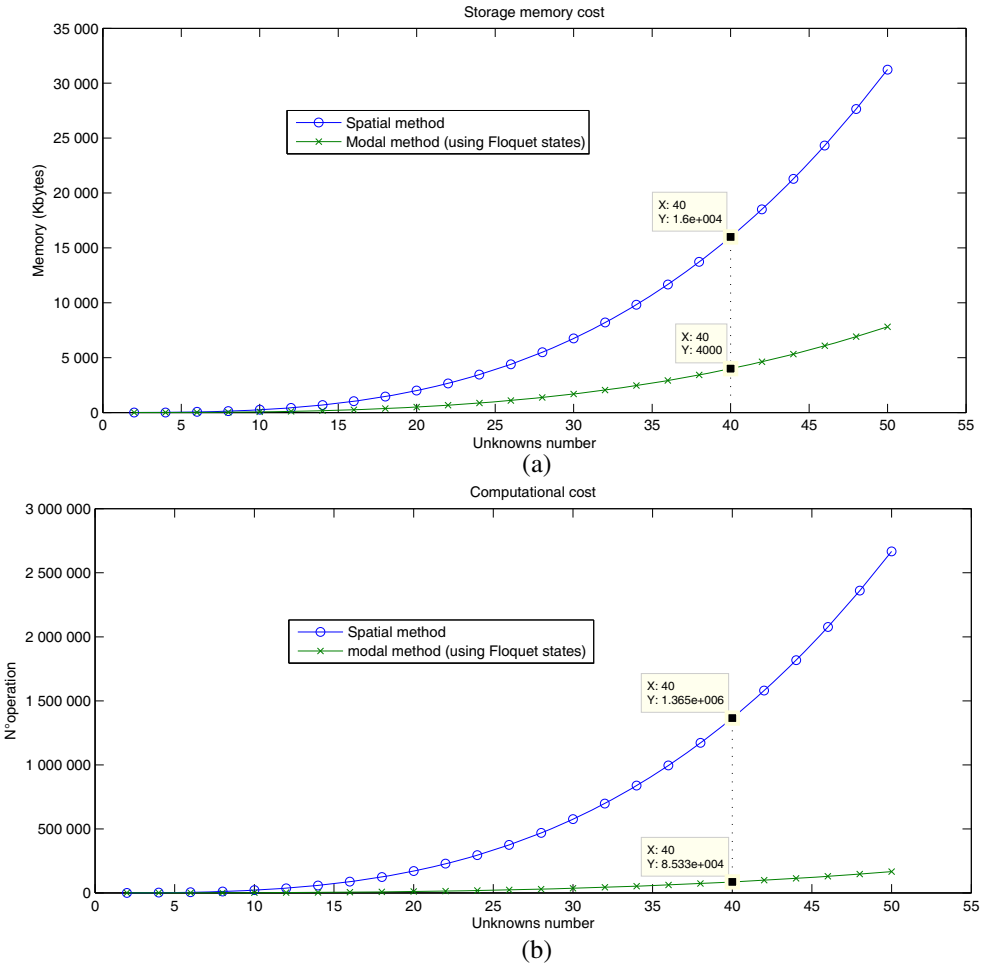

Figure 9. Computational cost versus the number of unknowns (2D-structure).

According to this study, the proposed formulations are applied to a (2×2) elements array: From Figure 9, we can see that the increase of the unknowns number will produce a great increase of the operation number by using the spatial formulation. So, the manipulated matrix requires a huge memory resources when unknowns grow. Whereas, in modal formulation these memory resources and operation number can be minimized significantly. As a result, the Floquet analysis with the modal representation is more adequate to study the large finite array which can be extended to an infinite array [1, 12, 26].

6. CONCLUSION

In this paper we present a new modal approach for the fast and efficient calculation of mutual coupling in planar periodic structures. It is important to show that the modal decomposition to study and analyze finite and infinite periodic structures successfully removes the complexity of the proposed problem.

For example, the employed formalism based on Floquet analysis reduces the electromagnetic calculation on one unit cell, in contrast to old methods to study the wave behavior of the whole structure. This allows an easier computation of the scattering matrix, by using a simple elegant Fourier Transformation.

The essential advantage of this new modal analysis is reducing computing time and memory requirement which are roughly proportional to the square or cube of the number of array elements.

Moreover, this original way permits to study different periodic and aperiodic configurations with distinct sources amplitudes.

In conclusion, we would like to highlight that Floquet analysis is needed to study many novel applications that open various areas of research.

APPENDIX A.

Matlab's code to express the drawn 1-D Fourier Matrix and 2-D Fourier Matrix according to the matrix-vector notation (with respect to their fundamental properties and the used indices):

(i) 1-D Fourier Matrix:

```
function FFT_1D = calcul_FFT_1D(N_x)
% 1-D Finite Fourier Matrix
% N_x elements number along x axis
if (rem(N_x,2)==0)%(even case)
omega = exp(-2*pi*i/N_x);% a complex nth root of unity
j =-(N_x/2):1:(N_x/2)-1;% position indices (along x direction)
k = j';% Floquet states
FFT_1D= omega.^(k*j);% Fourier Matrix
else %(odd case)
omega = exp(-2*pi*i/N_x);
j =-((N_x-1)/2):1:((N_x+1)/2)-1;%  position indices (along x direction)
k = j' ;% Floquet states
FFT_1D = omega.^(k*j);% Fourier Matrix
end
```

(ii) 2-D Fourier Matrix (see the next page):

APPENDIX B.

New basis functions (guide's modes) combine periodic walls with magnetic and electric walls to study 1-D periodic planar structure:

(i) Electric-Periodic boundary conditions (EPEP): (see [1])

$$\left\{ \begin{array}{l} |TE_{mn,\alpha}\rangle \\ m \in Z \\ n \in N^* \end{array} \right\} = \left\{ \begin{array}{l} \dfrac{k_{yn}}{\sqrt{k_{xm,\alpha}^2 + k_{yn}^2}} \sqrt{\dfrac{2}{dL}} \\ \exp(+j(k_{xm,\alpha}x)) \sin(k_{yn}y) \\ j \dfrac{k_{xm,\alpha}}{\sqrt{k_{xm,\alpha}^2 + k_{yn}^2}} \sqrt{\dfrac{2}{dL}} \\ \exp(+j(k_{xm,\alpha}x)) \cos(k_{yn}y) \end{array} \right. \tag{B1}$$

$$\left\{ \begin{array}{l} |TE_{m0,\alpha}\rangle \\ m \in Z^* \\ n = 0 \end{array} \right\} = \left\{ \begin{array}{l} 0 \\ j \sqrt{\dfrac{1}{dL}} \exp(+j(k_{xm,\alpha}x)) \end{array} \right. \tag{B2}$$

```
function FFT_2D = calcul_FFT_2D(N_x,N_y)
% 2-D Finite Fourier Matrix
% N_x elements number along x axis
% N_y elements number along y axis
if (rem(N_x,2)==0)%(even case)
omega_x = exp(-2*pi*i/N_x);% a complex nth root of unity
j =-(N_x/2):1:(N_x/2)-1;%  position indices (along x direction)
k = j';% Floquet states
FFT_x = omega_x.^(k*j);%Fourier Matrix (x dependance)
else%(odd case)
omega_x = exp(-2*pi*i/N_x);% a complex nth root of unity
j =-((N_x-1)/2):1:((N_x+1)/2)-1;%  position indices (along x direction)
k = j' ;% Floquet states
FFT_x = omega_x.^(k*j) ;%Fourier Matrix (x dependance)
end
if (rem(N_y,2)==0)%(even case)
omega_y = exp(-2*pi*i/N_y);% a complex nth root of unity
s=-(N_y/2):1:(N_y/2)-1;%  position indices (along y direction)
t= j';% Floquet states
FFT_y = omega_y.^(t*s);%Fourier Matrix (y dependance)
else%(odd case)
omega_y = exp(-2*pi*i/N_y);% a complex nth root of unity
s=-((N_y-1)/2):1:((N_y+1)/2)-1;%  position indices (along y direction)
t= j' ;% Floquet states
FFT_y= omega_y.^(t*s) ;%Fourier Matrix (y dependance)
end
for q=1:N_y
for p=1:N_y
FFT_2D((1+(p-1)*N_x):p*N_x,(1+(q-1)*N_x):q*N_x)=FFT_x*FFT_y(p,q);% 2-D Fourier Matrix
end
end
```

$$\left\{ \begin{array}{l} |TEM_{\alpha}\rangle \\ m=0 \\ n=0 \end{array} \right\} = \left\{ \begin{array}{l} |TE_{00,\alpha}\rangle \\ m=0 \\ n=0 \end{array} \right\} = \left\{ \begin{array}{l} 0 \\ j\sqrt{\dfrac{1}{dL}}\exp(+j(\alpha x)) \end{array} \right. \tag{B3}$$

$$\left\{ \begin{array}{l} |TM_{mn,\alpha}\rangle \\ m \in Z \\ n \in N^{*} \end{array} \right\} = \left\{ \begin{array}{l} \dfrac{-k_{xm,\alpha}}{\sqrt{k_{xm,\alpha}^2+k_{yn}^2}}\sqrt{\dfrac{2}{dL}} \\ \exp(+j(k_{xm,\alpha}x))\sin(k_{yn}y) \\ j\dfrac{k_{yn}}{\sqrt{k_{xm,\alpha}^2+k_{yn}^2}}\sqrt{\dfrac{2}{dL}} \\ \exp(+j(k_{xm,\alpha}x))\cos(k_{yn}y) \end{array} \right. \tag{B4}$$

$|TM_{m0,\alpha}\rangle$ and $|TM_{00,\alpha}\rangle$ do not exist.

$k_{xm,\alpha} = \frac{2m\pi}{d} + \alpha$ and $k_{yn} = \frac{n\pi}{L}$ are wavenumbers.

(ii) Magnetic-Periodic boundary conditions (MPMP): (see [23])

$$\left\{ \begin{array}{l} |TE_{mn,\alpha}\rangle \\ m \in Z \\ n \in N^{*} \end{array} \right\} = \left\{ \begin{array}{l} \dfrac{k_{yn}}{\sqrt{k_{xm,\alpha}^2+k_{yn}^2}}\sqrt{\dfrac{2}{dL}} \\ \exp(+j(k_{xm,\alpha}x))\cos(k_{yn}y) \\ -j\dfrac{k_{xm,\alpha}}{\sqrt{k_{xm,\alpha}^2+k_{yn}^2}}\sqrt{\dfrac{2}{dL}} \\ \exp(+j(k_{xm,\alpha}x))\sin(k_{yn}y) \end{array} \right. \tag{B5}$$

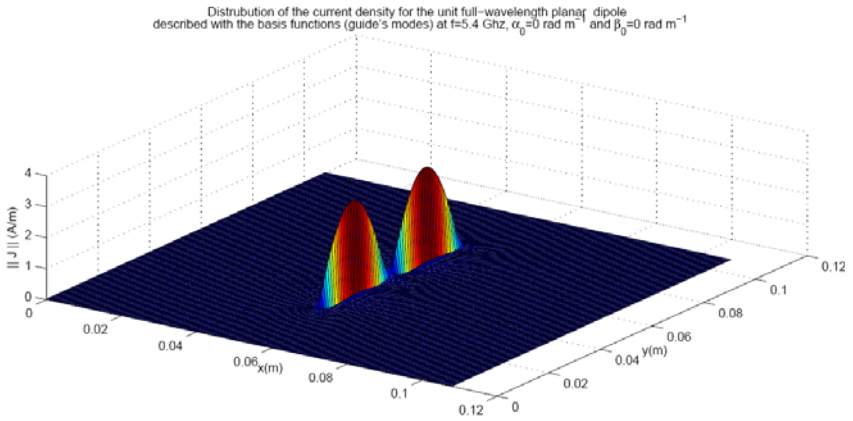

Figure B1. 2-D representation of the current density ($\frac{A}{m}$) for the unit full-wavelength planar dipole described with the basis functions (guide's modes) at $f = 5.4\,\text{GHz}$ and ($\alpha_0 = 0$ rad m^{-1}, $\beta_0 = 0\,\text{rad}$ m^{-1}): $w = 1\,\text{mm}$, $\delta = 0.75\,\text{mm}$ ($w \ll \lambda_0$, $\delta \ll \lambda_0$), $d_x = d_y \approx 2\lambda_0 \approx 108\,\text{mm}$, $L = \lambda_0 \approx 54\,\text{mm}$, $h = 1.25\,\text{mm}$ and $\epsilon_r = 1$ (air).

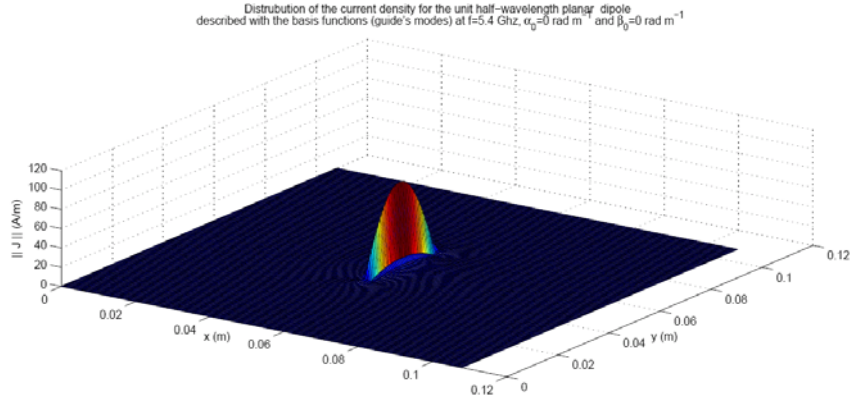

Figure B2. 2-D representation of the current density ($\frac{A}{m}$) for the unit half-wavelength planar dipole described with the basis functions (guide's modes) at $f = 5.4\,\text{GHz}$ and ($\alpha_0 = 0$ rad m^{-1}, $\beta_0 = 0\,\text{rad}$ m^{-1}): $w = 1\,\text{mm}$, $\delta = 0.75\,\text{mm}$ ($w \ll \lambda_0$, $\delta \ll \lambda_0$), $d_x = d_y \approx 2\lambda_0 \approx 108\,\text{mm}$, $L = \frac{\lambda_0}{2} \approx 27\,\text{mm}$, $h = 1.25\,\text{mm}$ and $\epsilon_r = 1$ (air).

$$\left\{ \begin{array}{l} |TM_{mn,\alpha}\rangle \\ m \in Z \\ n \in N^* \end{array} \right\} = \left\{ \begin{array}{l} \dfrac{-k_{xm,\alpha}}{\sqrt{k_{xm,\alpha}^2 + k_{yn}^2}} \sqrt{\dfrac{2}{dL}} \\ \exp(+j(k_{xm,\alpha}x)) \cos(k_{yn}y) \\ -j \dfrac{k_{yn}}{\sqrt{k_{xm,\alpha}^2 + k_{yn}^2}} \sqrt{\dfrac{2}{dL}} \\ \exp(+j(k_{xm,\alpha}x)) \sin(k_{yn}y) \end{array} \right. \tag{B6}$$

$$\left\{ \begin{array}{l} |TM_{m0,\alpha}\rangle \\ m \in Z^* \\ n = 0 \end{array} \right\} = \left\{ \begin{array}{l} -\sqrt{\dfrac{1}{dL}} \exp(+j(k_{xm,\alpha}x)) \\ 0 \end{array} \right. \tag{B7}$$

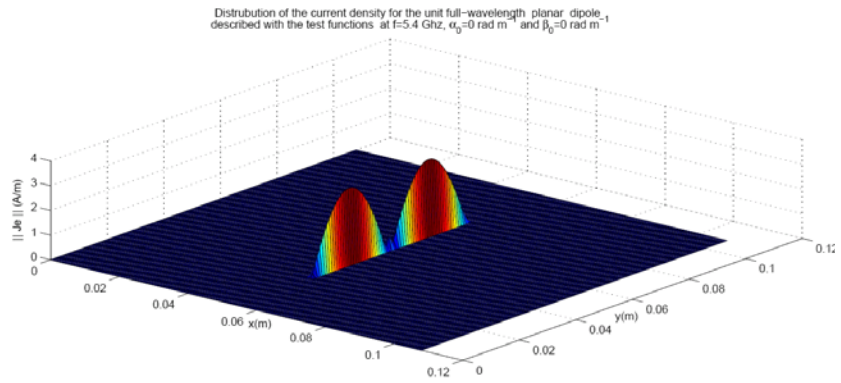

Figure B3. 2-D representation of the current density ($\frac{A}{m}$) for the unit full-wavelength planar dipole described with the trial functions at $f = 5.4\,\text{GHz}$ and ($\alpha_0 = 0$ rad m^{-1}, $\beta_0 = 0\,\text{rad m}^{-1}$): $w = 1\,\text{mm}$, $\delta = 0.75\,\text{mm}$ ($w \ll \lambda_0$, $\delta \ll \lambda_0$), $d_x = d_y \approx 2\lambda_0 \approx 108\,\text{mm}$, $L = \lambda_0 \approx 54\,\text{mm}$, $h = 1.25\,\text{mm}$ and $\epsilon_r = 1$ (air).

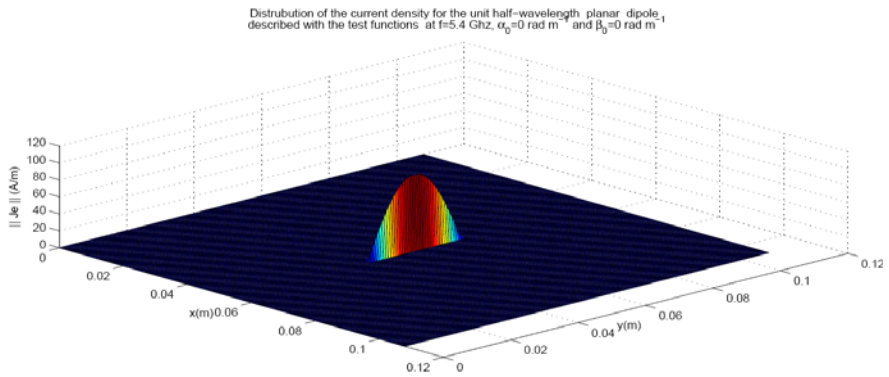

Figure B4. 2-D representation of the current density ($\frac{A}{m}$) for the unit half-wavelength planar dipole described with the trial functions at $f = 5.4\,\text{GHz}$ and ($\alpha_0 = 0$ rad m^{-1}, $\beta_0 = 0\,\text{rad m}^{-1}$): $w = 1\,\text{mm}$, $\delta = 0.75\,\text{mm}$ ($w \ll \lambda_0$, $\delta \ll \lambda_0$), $d_x = d_y \approx 2\lambda_0 \approx 108\,\text{mm}$, $L = \frac{\lambda_0}{2} \approx 27\,\text{mm}$, $h = 1.25\,\text{mm}$ and $\epsilon_r = 1$ (air).

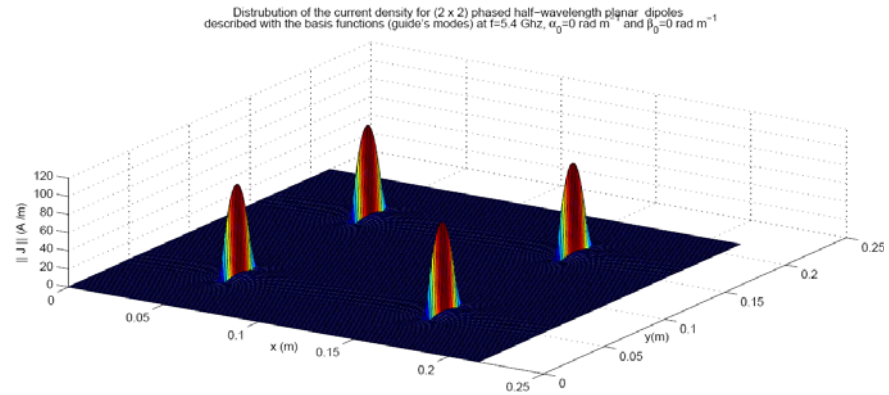

Figure B5. 2-D representation of the current density ($\frac{A}{m}$) for (2×2) phased half-wavelength planar dipoles described with the basis functions (guide's modes) at $f = 5.4\,\text{GHz}$, $\alpha_0 = 0\,\text{rad m}^{-1}$, $\beta_0 = 0\,\text{rad m}^{-1}$, $w = 1\,\text{mm}$, $\delta = 0.75\,\text{mm}$ ($w \ll \lambda_0$, $\delta \ll \lambda_0$), $d_x = 108\,\text{mm}$, $d_y = 108\,\text{mm}$, $L = \frac{\lambda_0}{2} \approx 27\,\text{mm}$, $h = 1.25\,\text{mm}$ and $\epsilon_r = 1$ (air).

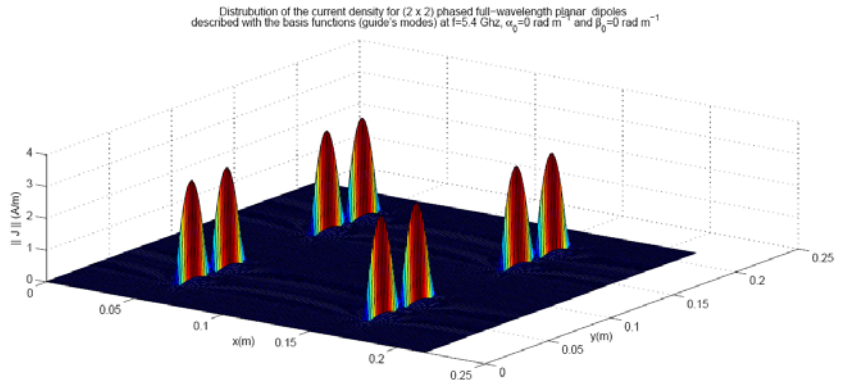

Figure B6. 2-D representation of the current density ($\frac{A}{m}$) for (2×2) phased full-wavelength planar dipoles described with the basis functions (guide's modes) at $f = 5.4\,\text{GHz}$, $\alpha_0 = 0\,\text{rad m}^{-1}$, $\beta_0 = 0\,\text{rad m}^{-1}$, $w = 1\,\text{mm}$, $\delta = 0.75\,\text{mm}$ ($w \ll \lambda_0$, $\delta \ll \lambda_0$), $d_x = 108\,\text{mm}$, $d_y = 108\,\text{mm}$, $L = \lambda_0 \approx 54\,\text{mm}$, $h = 1.25\,\text{mm}$ and $\epsilon_r = 1$ (air).

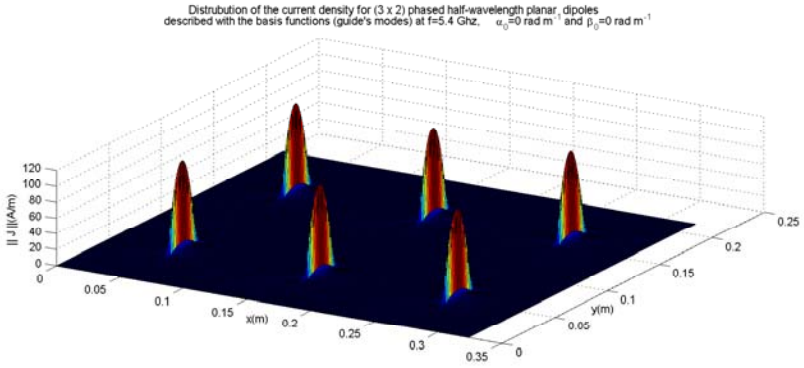

Figure B7. 2-D representation of the current density ($\frac{A}{m}$) for (3×2) phased half-wavelength planar dipoles described with the basis functions (guide's modes) at $f = 5.4\,\text{GHz}$, $\alpha_0 = 0\,\text{rad m}^{-1}$, $\beta_0 = 0\,\text{rad m}^{-1}$, $w = 1\,\text{mm}$, $\delta = 0.75\,\text{mm}$ ($w \ll \lambda_0$, $\delta \ll \lambda_0$), $d_x = 108\,\text{mm}$, $d_y = 108\,\text{mm}$, $L = \frac{\lambda_0}{2} \approx 27\,\text{mm}$, $h = 1.25\,\text{mm}$ and $\epsilon_r = 1$ (air).

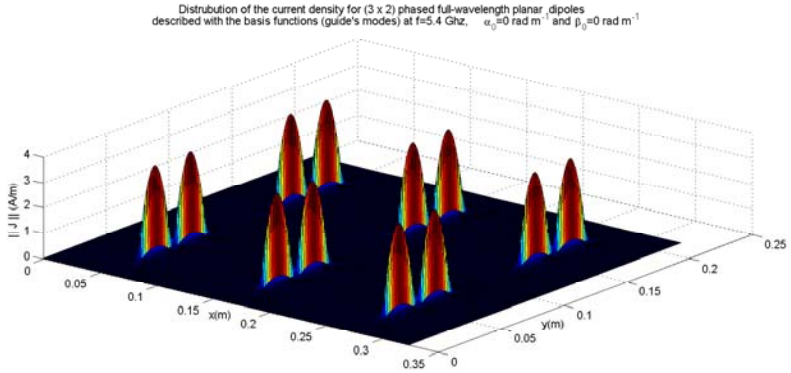

Figure B8. 2-D representation of the current density ($\frac{A}{m}$) for (3×2) phased full-wavelength planar dipoles described with the basis functions (guide's modes) at $f = 5.4\,\text{GHz}$, $\alpha_0 = 0\,\text{rad m}^{-1}$, $\beta_0 = 0\,\text{rad m}^{-1}$, $w = 1\,\text{mm}$, $\delta = 0.75\,\text{mm}$ ($w \ll \lambda_0$, $\delta \ll \lambda_0$), $d_x = 108\,\text{mm}$, $d_y = 108\,\text{mm}$, $L = \lambda_0 \approx 54\,\text{mm}$, $h = 1.25\,\text{mm}$ and $\epsilon_r = 1$ (air).

r

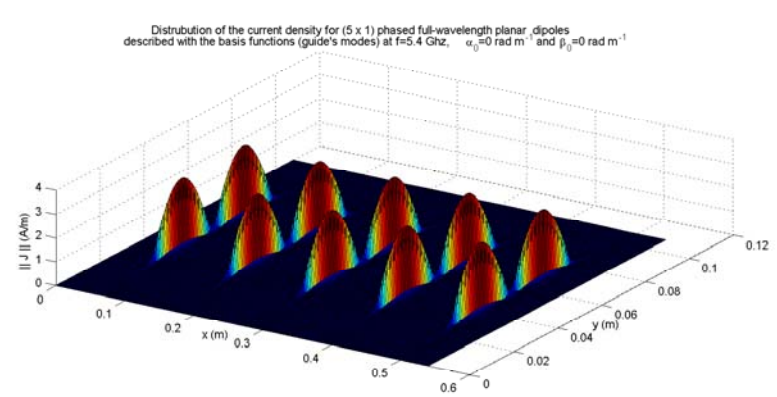

Figure B9. 2-D representation of the current density ($\frac{A}{m}$) for (5×1) phased full-wavelength planar dipoles described with the basis functions (guide's modes) at $f = 5.4\,\text{GHz}$, $\alpha_0 = 0\,\text{rad m}^{-1}$, $\beta_0 = 0\,\text{rad m}^{-1}$, $w = 1\,\text{mm}$, $\delta = 0.75\,\text{mm}$ ($w \ll \lambda_0$, $\delta \ll \lambda_0$), $d_x = 108\,\text{mm}$, $d_y = 108\,\text{mm}$, $L = \lambda_0 \approx 54\,\text{mm}$, $h = 1.25\,\text{mm}$ and $\epsilon_r = 1$ (air).

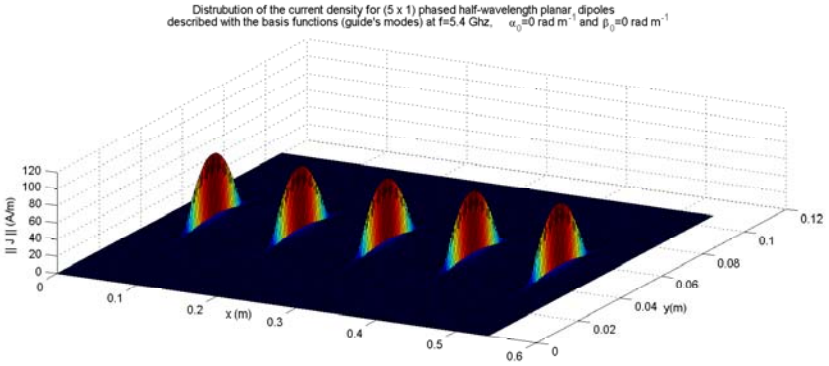

Figure B10. 2-D representation of the current density ($\frac{A}{m}$) for (5×1) phased half-wavelength planar dipoles described with the basis functions (guide's modes) at $f = 5.4\,\text{GHz}$, $\alpha_0 = 0\,\text{rad m}^{-1}$, $\beta_0 = 0\,\text{rad m}^{-1}$, $w = 1\,\text{mm}$, $\delta = 0.75\,\text{mm}$ ($w \ll \lambda_0$, $\delta \ll \lambda_0$), $d_x = 108\,\text{mm}$, $d_y = 108\,\text{mm}$, $L = \frac{\lambda_0}{2} \approx 27\,\text{mm}$, $h = 1.25\,\text{mm}$ and $\epsilon_r = 1$ (air).

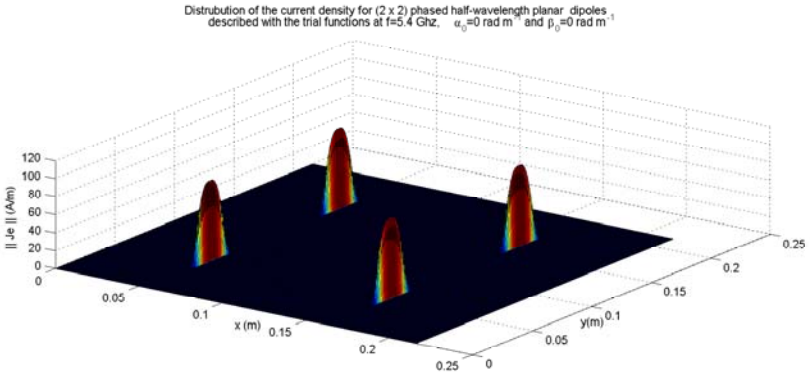

Figure B11. 2-D representation of the current density ($\frac{A}{m}$) for (2×2) phased half-wavelength planar dipoles described with the trial functions at $f = 5.4\,\text{GHz}$, $\alpha_0 = 0\,\text{rad m}^{-1}$, $\beta_0 = 0\,\text{rad m}^{-1}$, $w = 1\,\text{mm}$, $\delta = 0.75\,\text{mm}$ ($w \ll \lambda_0$, $\delta \ll \lambda_0$), $d_x = 108\,\text{mm}$, $d_y = 108\,\text{mm}$, $L = \frac{\lambda_0}{2} \approx 27\,\text{mm}$, $h = 1.25\,\text{mm}$ and $\epsilon_r = 1$ (air).

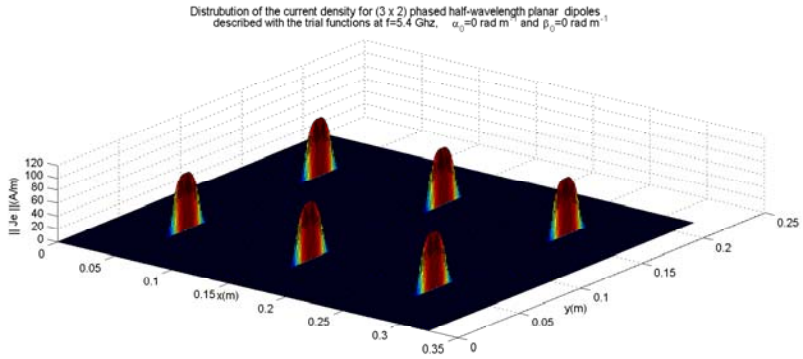

Figure B12. 2-D representation of the current density ($\frac{A}{m}$) for (3×2) phased half-wavelength planar dipoles described with the trial functions at $f = 5.4\,\text{GHz}$, $\alpha_0 = 0\,\text{rad m}^{-1}$, $\beta_0 = 0\,\text{rad m}^{-1}$, $w = 1\,\text{mm}$, $\delta = 0.75\,\text{mm}$ ($w \ll \lambda_0$, $\delta \ll \lambda_0$), $d_x = 108\,\text{mm}$, $d_y = 108\,\text{mm}$, $L = \frac{\lambda_0}{2} \approx 27\,\text{mm}$, $h = 1.25\,\text{mm}$ and $\epsilon_r = 1$ (air).

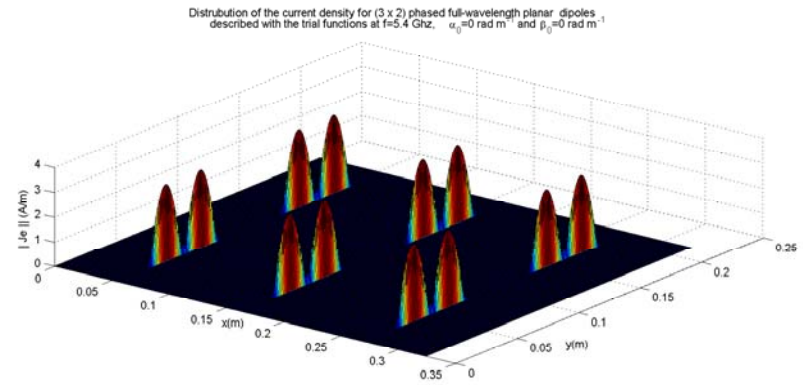

Figure B13. 2-D representation of the current density ($\frac{A}{m}$) for (3×2) phased full-wavelength planar dipoles described with the trial functions at $f = 5.4\,\text{GHz}$, $\alpha_0 = 0\,\text{rad m}^{-1}$, $\beta_0 = 0\,\text{rad m}^{-1}$, $w = 1\,\text{mm}$, $\delta = 0.75\,\text{mm}$ ($w \ll \lambda_0, \delta \ll \lambda_0$), $d_x = 108\,\text{mm}$, $d_y = 108\,\text{mm}$, $L = \lambda_0 \approx 54\,\text{mm}$, $h = 1.25\,\text{mm}$ and $\epsilon_r = 1$ (air).

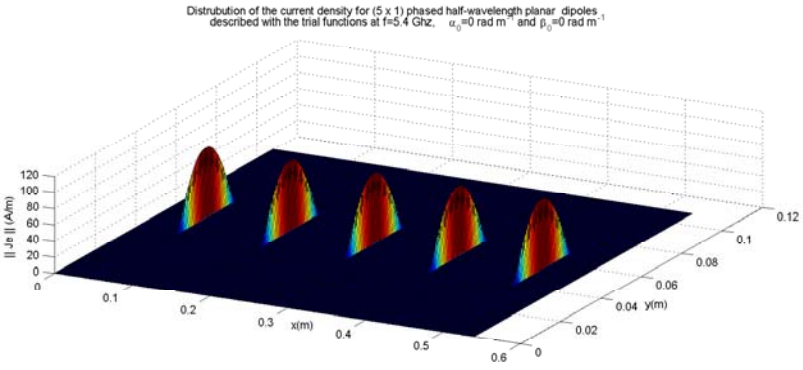

Figure B14. 2-D representation of the current density ($\frac{A}{m}$) for (5×1) phased half-wavelength planar dipoles described with the trial functions at $f = 5.4\,\text{GHz}$, $\alpha_0 = 0\,\text{rad m}^{-1}$, $\beta_0 = 0\,\text{rad m}^{-1}$, $w = 1\,\text{mm}$, $\delta = 0.75\,\text{mm}$ ($w \ll \lambda_0$, $\delta \ll \lambda_0$), $d_x = 108\,\text{mm}$, $d_y = 108\,\text{mm}$, $L = \frac{\lambda_0}{2} \approx 27\,\text{mm}$, $h = 1.25\,\text{mm}$ and $\epsilon_r = 1$ (air).

$$\left\{ \begin{array}{l} |TEM_{\alpha}\rangle \\ m=0 \\ n=0 \end{array} \right\} = \left\{ \begin{array}{l} |TM_{00,\alpha}\rangle \\ m=0 \\ n=0 \end{array} \right\} = \left\{ \begin{array}{l} -\sqrt{\dfrac{1}{dL}}\exp(+j(\alpha x)) \\ 0 \end{array} \right. \tag{B8}$$

The $|TE_{m0,\alpha}\rangle$ and $|TE_{00,\alpha}\rangle$ do not exist.
With $k_{xm,\alpha} = \frac{2m\pi}{d} + \alpha$ and $k_{yn} = \frac{n\pi}{L}$ are wavenumbers.

(iii) Electric-Periodic-Magnetic-Periodic boundary conditions (EPMP):

$$\left\{ \begin{array}{l} |TE_{mn,\alpha}\rangle \\ m \in Z \\ n \in N \end{array} \right\} = \left\{ \begin{array}{l} \dfrac{k_{yn}}{\sqrt{k_{xm,\alpha}^2 + k_{yn}^2}}\sqrt{\dfrac{2}{dL}} \\ \exp(+j(k_{xm,\alpha}x))\cos(k_{yn}y) \\ -j\dfrac{k_{xm,\alpha}}{\sqrt{k_{xm,\alpha}^2 + k_{yn}^2}}\sqrt{\dfrac{2}{dL}} \\ \exp(+j(k_{xm,\alpha}x))\sin(k_{yn}y) \end{array} \right. \tag{B9}$$

$$\left\{ \begin{array}{l} |TM_{mn,\alpha}\rangle \\ m \in Z \\ n \in N \end{array} \right\} = \left\{ \begin{array}{l} \dfrac{-k_{xm,\alpha}}{\sqrt{k_{xm,\alpha}^2 + k_{yn}^2}}\sqrt{\dfrac{2}{dL}} \\ \exp(+j(k_{xm,\alpha}x))\cos(k_{yn}y) \\ -j\dfrac{k_{yn}}{\sqrt{k_{xm,\alpha}^2 + k_{yn}^2}}\sqrt{\dfrac{2}{dL}} \\ \exp(+j(k_{xm,\alpha}x))\sin(k_{yn}y) \end{array} \right. \tag{B10}$$

With $k_{xm,\alpha} = \frac{2m\pi}{d} + \alpha$ and $k_{yn} = \frac{(\frac{2n+1}{2})\pi}{L}$ are wavenumbers.

REFERENCES

1. Hamdi, B., T. Aguili, N. Raveu, and H. Baudrand, "Calculation of the mutual coupling parameters and their effects in 1-D planar almost periodic structures," *Progress In Electromagnetics Research B*, Vol. 59, 269–289, 2014.
2. Ishimaru, A., R. J. Coe, G. E. Miller, and W. P. Green, "Finite periodic structure approach to large scanning array problems," *IEEE Trans. Antennas Propagat.*, 1985.
3. Mekkioui, Z. and H. Baudrand, "2-D bi-periodic centered-fed microstrip leaky-wave antenna (LWA) analysis by a source modal decomposition in spectral domain," *IET*, 2009.
4. Baudrand, H., M. Titaouine, N. Raveu, and G. Fontgland, "Electromagnetic modeling of planar almost periodic structures," *SBMOI/IEEE MTT-S International Microwave and Optoelectronics Conference*, 2009.
5. Hamdi, B., T. Aguili, and H. Baudrand, "Uni-dimensional planar almost periodic structures analysis to decompose central arbitrary located source in spectral domain," *IEEE-ANTEM 2012: 15th International Symposium of Antenna Technology and Applied ElectroMagnetics*, Toulouse, France.
6. Eleftheriades, G. V. and J. R. Mosig, "On the network characterization of planar passive circuits using the method of moments," *IEEE Transaction on Microwave Theory and Technoques*, Vol. 44, No. 3, March 1996.
7. Bhattacharyya, K. A., *Phased Array Antennas: Floquet Analysis, Synthesis, BFNs, and Active Array Systems*, Wiley and Sons, March 2006.
8. Xi, Y. P., D. G. Fang, Y. X. Sun, and Y. L. Chow, "Mutual coupling in a linear dipole array of finite size," *IEEE Proc.-Microw. Antennas Propag.*, Vol. 152, No. 5, October 2005.

9. Valerio, G., P. Baccarelli, P. Burghignoli, A. Galli, R. Rodrguez-Berral, and F. Mesa, "Analysis of periodic shielded microstrip lines excited by nonperiodic sources through the array scanning method," *Radio Science*, Vol. 43, 2008.
10. Azizi, M. K., L. Latrach, N. Raveu, A. Gharsallah, and H. Baudrand, "A new approach of almost periodic lumped elements circuits by an iterative method using auxiliary sources," *American Journal of Applied Sciences*, Vol. 10, No. 11, 1457–1472, 2013.
11. Watanabe, K. and K. Yasumoto, "Two-dimensional electromagnetic scattering of non-plane incident waves by periodic structures," *Progress In Electromagnetics Research*, Vol. 74, 241–271, 2007.
12. Mili, S., C. L. Aguili, and T. Aguili, "Study of fractal-shaped structures with pin diodes using the multi-scale method combined to the generalized equivalent circuit modeling," *Progress In Electromagnetics Research B*, Vol. 27, 213–233, 2011.
13. Rodrguez-Berral, R., F. Mesa, P. Baccarelli, and P. Burghignoli, "Excitation of a periodic microstrip line by an aperiodic delta-gap source," *IEEE Trans. Antennas Propagat. Letters*, Vol. 8, 2009.
14. Watanabe, K., "Spectral-domain approach to electromagnetic scattering from imperfectly periodic," *13th International Conference on Mathematical Methods in Electromagnetic Theory*, Ukraine, September 2010.
15. Abdallah, Y., C. Menudier, M. Thevenot, and T. Monediere, "Investigations of the effects of mutual coupling in reflectarray antennas" *IEEE Antennas and Propagation Magazine*, Vol. 55, No. 2, April 2013.
16. Skrivervik, K. and L. R. Mosig, "Finite phased array of microstrip patch antennas: The infinite array approach," *IEEE Trans. Antennas Propagat.*, 1992.
17. Craeye, C. and D. G. Ovejero, "A review on array mutual coupling analysis," *Radio Science*, Vol. 46, RS2012, doi:10.1029/2010RS004518, 2011.
18. Baudrand, H., *Circuits Passifs en Hyperfréquences*, Editions Cépaduès, Janvier, 2001.
19. BenSalah, T., C. L. Aguili, and T. Aguili, "Renormalization group application to multi-port model for studying fractal-shaped structures' diffraction," *PIERS Proceedings*, 1629–1633, Beijing, China, March 23–27, 2009.
20. Makarov, S., A. Puzella, and V. Iyer, "Scan impedance for an infinite dipole array: Accurate theoretical model compared to numerical software," *IEEE Antennas and Propagation Magazine*, Vol. 50, December 2008.
21. Massaro, A., R. Cingolani, A. Passaseo, and M. De. Vittoriol, "Floquet's unit cell design for periodic structures at optical frequencies," *International Journal of Microwave Science and Technology*, 10 pages, Article ID 160321, 2009.
22. Vardaxoglou, J. C., *Frequency Selective Surfaces, Analysis and Design*, John Wiley and Sons, 1997.
23. Mekkioui, Z. and H. Baudrand, "A full-wave analysis of uniform microstrip leaky-wave antenna with arbitrary metallic strips," *Electromagnetics*, Vol. 28, No. 4, 296–314, 2008.
24. Riabi, M. L., M. Ahmadpanah, H. Benzina, H. Baudrand, and V. F. Hanna, "Performance of the LSBRM using efficient weighting functions for planar structures," *IEEE Trans. Antennas Propagat.*, August 1995.
25. Aguili, T., "Modélisation des composants S. H. F planaires par la méthode des circuits équivalents généralisés," Thesis, National Engineering School of Tunis ENIT, May 2000.
26. Sultan, K. S., H. H. Abdullah, and E. A. Abdallah, "Method of moments analysis for antenna arrays with optimum memory and time consumption," *PIERS Proceedings*, 1353–1356, Kuala Lumpur, Malaysia, March 27–30, 2012.
27. Li, D. and C. D. Sarris, "Efficient finite-difference time-domain modeling of periodicstructures under non-periodic sources," *Antennas and Propagation Society International Symposium*, 2007.
28. Raveu, N. and O. Pigaglio, "Résolution de problèmes hautes fréquences par les schémas équivalents," Éditions Cépaduès, Mai 2012.